

# The WARPS Survey: VI. Galaxy Cluster and Source Identifications from Phase I

Eric S. Perlman<sup>1,7,9,11,12,13,14,15</sup>, Donald J. Horner<sup>2,8,11,12</sup>, Laurence R. Jones<sup>3,11,13,14,15</sup>, Caleb A. Scharf<sup>1,10,12</sup>, Harald Ebeling<sup>4,13,14,16</sup>, Gary Wegner<sup>5,17</sup>, and Matthew Malkan<sup>6,15</sup>

## ABSTRACT

---

<sup>1</sup>Space Telescope Science Institute, 3700 San Martin Drive, Baltimore, MD 21218, USA

<sup>2</sup>Laboratory for High Energy Astrophysics, Code 662, Goddard Space Flight Center, Greenbelt, MD 20771, USA

<sup>3</sup>School of Physics & Astronomy, University of Birmingham, Birmingham B15 2TT, UK

<sup>4</sup>Institute for Astronomy, 2680 Woodlawn Drive, Honolulu, HI 96822, USA

<sup>5</sup>Department of Physics and Astronomy, Dartmouth College, 6127 Wilder Laboratory, Hanover, NH 03755, USA

<sup>6</sup>Department of Physics and Astronomy, University of California, Los Angeles, CA 90024, USA

<sup>7</sup>Department of Physics and Astronomy, Johns Hopkins University, 3400 North Charles Street, Baltimore, MD 21218, USA

<sup>8</sup>Department of Astronomy, University of Maryland, College Park, MD 20742, USA

<sup>9</sup>Department of Physics, University of Maryland - Baltimore County, 1000 Hilltop Circle, Baltimore, MD 21250, USA

<sup>10</sup>Columbia Astrophysics Laboratory, Columbia University, Mail Code 5247, 550 West 120th Street, New York, NY 10027, USA

<sup>11</sup>Guest Observer at Kitt Peak National Observatory. KPNO/NOAO is operated by the Association of Universities for Research in Astronomy (AURA), Inc. under cooperative agreement with the National Science Foundation

<sup>12</sup>Guest Observer at Cerro Tololo Inter-American Observatory. CTIO is operated by the Association of University for Research in Astronomy (AURA), Inc. under cooperative agreement with the National Science Foundation

<sup>13</sup>Guest Observer at the Canada-France-Hawaii Telescope. CFHT is operated by the National Research Council of Canada, the Centre National de la Recherche Scientifique de France, and the University of Hawaii

<sup>14</sup>Guest Observer at the W. M. Keck Observatory. The W.M. Keck Observatory is operated as a scientific partnership among the California Institute of Technology, the University of California and the National Aeronautics and Space Administration.

<sup>15</sup>Guest Observer at Lick Observatories. Lick Observatory is operated by the University of California.

<sup>16</sup>Observer at the University of Hawaii 2.2m telescope on Mauna Kea.

<sup>17</sup>Observer at the Michigan-Dartmouth-MIT Observatory.

We present in catalog form the optical identifications for objects from the first phase of the Wide Angle ROSAT Pointed Survey (WARPS). WARPS is a serendipitous survey of relatively deep, pointed ROSAT observations for clusters of galaxies. The X-ray source detection algorithm used by WARPS is Voronoi Tessellation and Percolation (VTP), a technique which is equally sensitive to point sources and extended sources of low surface brightness. WARPS-I is based on the central regions of 86 ROSAT PSPC fields, covering an area of 16.2 square degrees. We describe here the X-ray source screening and optical identification process for WARPS-I, which yielded 34 clusters at  $0.06 < z < 0.75$ . Twenty-two of these clusters form a complete, statistically well defined sample drawn from 75 of these 86 fields, covering an area of 14.1 square degrees, with a flux limit of  $F(0.5 - 2.0 \text{ keV}) = 6.5 \times 10^{-14} \text{ erg cm}^{-2} \text{ s}^{-1}$ . This sample can be used to study the properties and evolution of the gas, galaxy and dark matter content of clusters, and to constrain cosmological parameters. We compare in detail the identification process and findings of WARPS to those from other recently published X-ray surveys for clusters, including RDCS, SHARC-Bright, SHARC-south and the CfA 160 deg<sup>2</sup> survey. The number counts and cluster IDs are found to agree quite well for all surveys except SHARC-Bright, for which we find persuasive evidence for incompleteness at the 30-40% level.

## 1. Introduction

Clusters of galaxies represent the largest gravitationally bound structures in the universe. Their space density and evolution strongly constrain hierarchical structure formation models, which postulate that the most massive clusters form via mergers of less massive clusters. The measurement of the X-ray temperature and luminosity functions (XTF and XLF) of clusters of galaxies are powerful discriminants between hierarchical models of structure formation (e.g., Kaiser 1991), which can provide strong constraints on cosmological models (e.g., Bahcall & Cen 1992; Viana & Liddle 1996; Carlberg et al. 1997). In order to study the distribution of massive clusters in the universe, as well as their characteristics, it is crucial to compile large, relatively unbiased samples of clusters.

One of the least biased ways to select a sample of clusters with properties directly translatable to the size of the mass aggregation, is via X-ray surveys. The X-ray emission in clusters originates in primordial gas and material stripped from the galaxies in the clusters, and scales directly with the density and temperature of the emitting gas (Jones & Forman 1984), which in turn are strongly correlated with the gravitating mass (Horner et al. 1999).

Optical surveys, by comparison, are strongly affected by projection effects (Lucey 1983; Struble & Rood 1991; Sutherland 1988; Frenk et al. 1990; van Haarlem et al. 1997). Moreover, a number of studies have found that the optical properties of clusters (e.g., richness) are not very good indicators of cluster mass (Frenk et al. 1990).

The Wide-Angle ROSAT Pointed Survey (WARPS; Scharf et al. 1997, hereafter Paper I; Jones et al. 1998, hereafter Paper II; Ebeling et al. 2001b, hereafter Paper III; Fairley et al. 2000, hereafter Paper IV, Ebeling et al. 2001a, hereafter Paper V) was designed to compile a representative, X-ray selected sample of clusters of galaxies. Groups of galaxies and individual galaxies are also detectable in WARPS, to somewhat lower redshifts than clusters (out to  $z \sim 0.2 - 0.3$  and  $z \sim 0.05$ , respectively, compared to  $z > 1$  for clusters). WARPS uses the Voronoi Tessellation and Percolation (VTP, Ebeling 1993; Ebeling & Wiedenmann 1993) algorithm to detect both extended and point-like X-ray sources. Our application of VTP to detect X-ray sources has been described in Paper I, as has the survey calibration. An extensive optical follow-up program (described in detail in Paper II) imaged not only extended X-ray sources (which are the most promising cluster candidates) but also all blank field point X-ray sources, and then took spectra of galaxies in the fields of cluster candidates. We assume that groups and clusters of galaxies form a continuous population, referred to simply as “clusters,” and do not further distinguish between groups and clusters of galaxies.

Early measurements of the cluster XLF, based on EXOSAT data (Edge et al. 1990) and the *Einstein* Extended Medium Sensitivity Survey (EMSS, Henry et al. 1992), indicated strong negative evolution at  $L(0.3 - 3.5 \text{ keV}) > 10^{44} \text{ erg s}^{-1}$ , perhaps even at relatively low redshifts. This was seen as support for critical density, cold dark matter cosmologies (e.g., Viana & Liddle 1996). However, a large number of recent results have changed the picture substantially. At low redshift ( $z < 0.3$ ), the results of the ROSAT Brightest Cluster Sample (BCS, Ebeling et al. 1997) show little if any evolution of the cluster XLF. At higher redshift, both new ROSAT surveys (RDCS, Rosati et al. 1998; WARPS, Papers II, III; SHARC-south Burke et al. 1997; SHARC-Bright Romer et al. 2000; CfA 160 deg<sup>2</sup> [also known as VMF], Vikhlinin et al. 1998b; NEP, Mullis 2000) and re-analyses of EMSS data (Nichol et al. 1997, Stocke et al., in preparation) are again consistent with no evolution at  $z < 1$  (except perhaps at the highest luminosities; see in particular Rosati et al. 1998; Vikhlinin et al. 1998a). The reason for this discrepancy is a subject of active debate, but contributing factors may include underestimation of X-ray flux by the EMSS (Papers II, III), and misidentification of some EMSS X-ray sources as clusters (Nichol et al. 1997; Rector et al. 1999). Indeed, the most current analysis of the highest-redshift part of the EMSS sample (Luppino & Gioia 1995) is also consistent with no significant evolution between  $z \sim 0.33$  and  $z \sim 0.75$  (see also Paper III; although for a somewhat different view of the same literature see Gioia et al. 2001).

Here we describe the identification process and and present in catalog form optical identifications for objects from the first phase of the WARPS project (WARPS-I), which included data from 86 ROSAT Position Sensitive Proportional Counter (PSPC) fields. This sample formed the basis of Papers I and II. The optical identifications for galaxy clusters from WARPS-I are essentially complete. Papers III, IV, and V also include data from the second phase of the WARPS project (WARPS-II), which includes nearly 4 times as many PSPC fields and concentrates on the most distant clusters. Those identifications are almost complete and will be presented elsewhere (Horner et al. in preparation).

In § 2 we describe briefly the survey methods and source identification process, as well as cross-correlations with various astronomical databases. In § 3 we comment explicitly on the efficacy of VTP as a method for detecting clusters of galaxies, and compare it with other X-ray source detection methods currently in use. In § 4 we describe the statistically complete, flux limited WARPS-I sample of clusters of galaxies, and also comment on individual clusters and interesting sources which fall below the flux limit. We conclude in § 5 by outlining future directions for research with this and other cluster samples.

Unless otherwise stated, we use  $q_0 = 0.5$  and  $H_0 = 50 \text{ km s}^{-1} \text{ Mpc}^{-1}$  when calculating distance dependent quantities. Similarly, we use the 0.5–2.0 keV ROSAT PSPC band when quoting count rates, fluxes, and luminosities unless otherwise noted. The catalogs, finder charts, and other information can be found on our WARPS WWW page at <http://lheawww.gsfc.nasa.gov/~horner/warpsI/warpsI.html>.

## 2. Survey Methods

The WARPS-I sample was drawn from 86 ROSAT PSPC pointings, covering a total area of  $16.2 \text{ deg}^2$ . These fields were selected at random from ROSAT observations with exposure times greater than 8 ks and Galactic latitude  $|b| > 20^\circ$ . Fields centered on bright star clusters or nearby bright galaxies such as M31 were excluded. This sample was used in Paper II. However, a more restrictive field selection has subsequently been applied to make WARPS-I consistent with WARPS-II. This selection process excluded 11 fields, so that the statistically complete sample is now drawn from 75 ROSAT fields ( $14.1 \text{ deg}^2$ ). Four fields (rp200510, rp400117, rp700257, and rp700302) were dropped due to their high background level. One field (rp600097) was discarded due to the presence of the large optical target, NGC 600. Five other fields (rp800003, rp800150a01, rp800401a01, rp800471n00, and rp800483n00) were dropped since the pointing targets are galaxy clusters. One ROSAT field originally included in the sample, rp700305, was subsequently split in the archive into two separate fields, rp700305a00 and rp700305a01, each with exposure time less than 8ks. Since

it is our policy not to combine fields, we have dropped this field from consideration. Any clusters found in the dropped fields as part of the optical follow-up are reported here, but they are not considered part of the statistically complete sample. In Table 1, we list all fields included in WARPS-I.

### 2.1. X-ray Source Detection

In each PSPC field we utilized the annulus between  $3'$  and  $15'$  radius. At the outer limit this ensures that the point-spread function (PSF), the size of which increases with radius, has a FWHM of  $< 45''$ , and also avoids areas strongly shaded by the PSPC window support structure. At the inner limit, this avoids the target of each pointing. We used only photons in the 0.5–2.0 keV band for source detection and measurement of fluxes. This minimizes both the size of the PSF and background relative to typical cluster spectra.

The VTP algorithm (Ebeling 1993; Ebeling & Wiedenmann 1993) was used for X-ray source detection. VTP is a general method for detecting non-Poissonian structure in a two-dimensional event distribution. In the case of detected photons, VTP will detect all regions of enhanced surface brightness. The implementation of VTP has previously been described in Papers I and II; here we discuss only the most important points.

The Voronoi tessellation is composed by defining each photon as the center of a cell polygon whose sides form the perpendicular bisectors of the non-crossing vectors joining the nearest neighbor photons. The surface brightness associated with this cell equals the number of photons in the cell (one, unless several photons were registered in the same PSPC resolution element) times the inverse of the product of cell area and local exposure time. To account for the non-uniform exposure of each PSPC field, we constructed exposure maps in two energy bands (0.5–0.9 and 0.9–2.0 keV), using an algorithm based on the work of Snowden et al. (1992). This resulted in an improvement of up to 10–15% in the computation of source fluxes. VTP then searches for brightness enhancements by comparing the cumulative surface brightness distribution with the expectation from a Poisson distribution, and finds a global threshold for the surface brightness distribution in a given field at which the observed distribution becomes inconsistent with random noise. In the percolation step of the VTP analysis, the algorithm groups into sources all adjacent cells whose surface brightness exceeds the threshold value. Sources consisting of very few photons consistent with random fluctuations are discarded; for the remainder VTP computes source properties, such as source position, count rate, and signal-to-noise ratio.

In using VTP, we set a lower limit in count rate of  $3 \times 10^{-3}$  ct/s for inclusion in the

preliminary sample, corresponding to a flux of approximately  $3.5 \times 10^{-14}$  ergs cm $^{-2}$  s $^{-1}$  in the 0.5–2.0 keV band. However, our final limit in *total flux* (*i.e.*, corrected for the component below our detection threshold) is  $6.5 \times 10^{-14}$  ergs cm $^{-2}$  s $^{-1}$  in the 0.5–2.0 keV band. This flux limit is slightly higher than that chosen in Paper II ( $6.0 \times 10^{-14}$  ergs cm $^{-2}$  s $^{-1}$ ) to be sure of completeness; it was chosen as a result of the simulations described in Paper I, which tested both the threshold at which we could reliably label a source as extended as well as the typical sizes of the flux corrections we applied for extended sources.

VTP was run five times on each field using different surface brightness thresholds in order to distinguish real single sources from those composed of blends of several sources (point-like or extended). This also reduces uncertainties in the count rate of sources close to, and occasionally blended with, positive background fluctuations. We then selected the optimal surface brightness threshold for each field by visually inspecting the VTP source photon distribution for each of the five thresholds. This procedure not only allowed us to separate sources blended together at low percolation thresholds, but also permitted us to identify and merge complex extended sources split into several fainter sources at high percolation thresholds (cf. §3).

The list of deblended sources and respective VTP parameters were then passed to an algorithm that estimates their true total flux. To do this, one must make assumptions about source morphology. We chose to assume that sources are either intrinsically point-like or follow a King profile with  $\beta = 2/3$ ; normalization and core radius are free parameters determined from the VTP source parameters. For each source, we then computed two flux estimates,  $S_{\text{King}}$  and  $S_{\text{point}}$ , under the above assumptions. We classify an object as extended if its extent parameter  $f_{\text{ext}}$ , defined as the ratio  $S_{\text{King}}/S_{\text{point}}$ , lies above 1.2, and “marginally extended” if  $1.1 < f_{\text{ext}} < 1.2$ .

In Table 2, we list all sources found by VTP with fluxes  $F_x \geq 6.5 \times 10^{-14}$  ergs cm $^{-2}$  s $^{-1}$ . Table 3 lists sources at lower fluxes and in fields that did not qualify for the complete sample. Optical images and spectra were not obtained for every X-ray source, as described in §2.2, so for the non-cluster candidates (*e.g.*, AGN, § 2.4) our identification process cannot be regarded as complete. Only 40% of all sources were identified either from the literature or through follow-up observations. The columns in Tables 2 and 3 are as follows:

1. The assigned source name.
2. The ROSAT pointing containing the source.
3. The right ascension (hours, minutes, seconds) in J2000 coordinates (typical error is 15'').

4. The declination (degrees, minutes, seconds) in J2000 coordinates (typical error is  $15''$ ).
5. The raw VTP count rate in units of  $10^{-3}$  counts per second.
6. The corrected (i.e., total) VTP count rate in units of  $10^{-3}$  counts per second.
7. The Galactic hydrogen column density ( $N_H$ ) in units of  $10^{20}$   $\text{cm}^{-2}$  from Dickey & Lockman (1990).
8. The unabsorbed X-ray flux in units of  $10^{-13}$   $\text{ergs cm}^{-2} \text{s}^{-1}$  in the 0.5–2.0 keV band. For clusters of galaxies, the flux was calculated using the same iterative method used by Ebeling et al. (1998). We assume a Raymond-Smith spectrum with a redshift appropriate for each cluster and metal abundance of 0.3 solar. The temperature of the model was derived iteratively by constraining the cluster to obey the observed  $L - T$  relation (White, Jones & Forman 1997). Fluxes were obtained for AGN and unidentified sources assuming a power law spectrum with  $F_\nu \propto \nu^{-1}$ . The flux for sources identified as stars was calculated assuming a Raymond-Smith model with a temperature of  $2 \times 10^6$  K and no correction for Galactic hydrogen column density.
9. The extent parameter as discussed above.
10. The imaging status of the source. The letter indicates the band of the optical image(s) obtained.
11. The status of the spectroscopic follow-up. A 'Y' indicates that spectra were taken for this source.
12. The identification of the source (e.g., cluster, AGN, star). Identifications in lower case were identified based on the literature (primarily using NED and SIMBAD) while upper case IDs are based on WARPS optical follow-up observations. Sources listed as blends are briefly discussed in the notes column.
13. The redshift of the source, if known, or spectral type for stars.
14. Alternate names and other notes. Sources listed as SHARC appear in the SHARC Bright Survey catalog (Romer et al. 2000). Sources listed as VMF correspond to sources in the CfA 160  $\text{deg}^2$  survey of Vikhlinin et al. (1998b). Sources listed as RIXOS correspond to sources in the RIXOS survey catalog (Mason et al. 2000). NVSS (Condon et al. 1998) and FIRST (e.g., White et al. 1997) radio sources are also indicated.

In Figure 2, we show overlays of the observed X-ray emission on digitized plates from the POSS-I, UKST, or POSS-II surveys for all 60 sources with  $F_x \geq 6.5 \times 10^{-14}$   $\text{ergs cm}^{-2} \text{s}^{-1}$ ,

that are within the complete sample fields and were flagged by VTP as either extended or marginally extended. We have also included at the end of the Figure, 4 additional X-ray sources which were classified as pointlike by VTP but were selected as cluster candidates based on optical imaging (§ 2.3.1). As discussed in §4, one of these four sources turned out to be a  $z = 0.722$  cluster. Finder charts for X-ray sources not identified as cluster candidates are available on our WWW page.

## 2.2. Optical/X-ray Selection of Cluster Candidates

In order to select sources for follow-up, it was necessary to define selection criteria for cluster candidates, as well as an integrated program of optical imaging and spectroscopy. This sub-section discusses the selection criteria, while the next sub-section discusses the optical follow-up program and how it was integrated with the selection criteria. In Paper II, we detailed the method by which we decided to image and take spectra of possible cluster candidates. Here we review the essential points.

### 2.2.1. Selection Criteria

The primary motivation for the selection criteria was to ensure the completeness of the sample of clusters of galaxies. In order to ensure maximal completeness, we followed up our deblending with a visual screening of every X-ray source. This is helpful because even after deblending, an X-ray source can have a large  $f_{ext}$  either by virtue of being truly extended or because it is a blend of two or more unresolved sources too close to be resolved by the ROSAT PSPC. It is also helpful because a finite probability exists for a truly extended source to masquerade as a point source in the VTP list, if for example it is either very core dominated (*e.g.*, an extreme cooling flow) or at very high redshifts. Finally, as noted above, sources of low surface brightness can be split up by deblending into multiple sources. Each of these effects is applicable not only to VTP but indeed to any algorithm of X-ray source detection, or any algorithm which determines source extent, as discussed in Paper II.

This procedure allowed us to sort the X-ray sources into four categories - (1) those flagged by VTP as extended which were very likely physically extended; (2) those flagged by VTP as extended which were very likely blends; (3) those flagged by VTP as point-like which were possibly extended; and (4) those flagged by VTP as point-like which were likely point-like. We then decided to accept for our first cut list of cluster candidates *every* source which might possibly be a cluster. This included not only all sources flagged by our source

detection procedure as extended or marginally extended (i.e., categories 1 and 2 above), but also a significant number of sources flagged as point-like (category 3 above).

Once a candidate source list was selected, we then designed an optical follow-up program which placed particular emphasis on both completeness and reliability. Included in this list were a number of sources which eventually fell below the flux limit. The reason for this is two-fold: first of all we wanted to compile a complete cluster list, so all extended sources in phase I were followed up regardless of whether they exceeded the flux limit; and second, as our processing algorithms improved, VTP was rerun, and thus the fluxes changed slightly.

To carry out our first screening, Automatic Plate Measuring Facility (APM; see Irwin et al. 1994) measurements of Palomar  $E$  and  $O$  and UKST  $R$  and  $B_j$  plates were obtained at the positions of all X-ray sources with count rate  $> 3 \times 10^{-3}$  ct/s (0.5–2 keV) within the survey area. We also obtained the Digitized Sky Survey images of the source fields, and overlaid X-ray contours. A large fraction of the X-ray sources have obvious optical counterparts which are immediately pinpointed in this step. This also allows one to identify systematic pointing errors, which can reach  $\sim 15''$  and varies in direction from dataset to dataset (Briel & Pfeffermann 1995). Once these overlays were made, a source was accepted as a possible cluster candidate if it met any one of three criteria:

- The X-ray source is extended or marginally extended and at least one galaxy is visible on the digitized sky survey plate, where the galaxy (ies) is not local ( $z \lesssim 0.01$ ) and of similar optical and X-ray size. In this case we not only obtained an image but immediately selected the field for spectroscopy.
- The X-ray source is extended or marginally extended and no optical counterpart is visible within one magnitude of the plate limit.
- The X-ray source is point-like but no optical counterpart is visible within one magnitude of the plate limit.

This process selected 108 sources for optical imaging. In practice some sources just below the flux limit were followed up because (a) the final fluxes depended to a small degree on the unknown source spectrum, which for clusters is based on the  $L - T$  relation and thus requires knowledge of the redshift, and (b) some source fluxes changed slightly at one point during the survey when we reran the VTP algorithm. Figure 1b shows a histogram of the extent parameters  $f_{ext}$  of the cluster candidates in the complete sample from this first screening.

### 2.2.2. *Cross-correlation with other source catalogs*

In order to identify previously known clusters, as well as AGN, Galactic stars and radio sources, we cross-correlated our source list with NED, SIMBAD and the NVSS and FIRST VLA survey lists (Condon et al. 1998, Becker et al. 1995). This produced a large number of IDs, particularly for non-cluster sources, which we list in Table 2 and 3. It also allowed us to screen out some X-ray sources we flagged as possibly extended, as more likely AGN. The cross-correlation with the NVSS revealed that 18 WARPS clusters may contain radio sources; the fluxes of these sources are listed in Table 6 (see also § 4). This is certainly not unexpected; both in the present epoch and at redshifts up to  $z = 0.8$ , approximately 30-50% of clusters contain radio galaxies, usually of the FR 1 type (Owen & Ledlow 1997; Stocke et al. 1999). In the case of optical clusters with radio sources in the field, we have checked the X-ray/optical overlays for X-ray enhancements and/or other evidence that some of the observed X-rays might be emitted by an AGN. Two such cases are noted in § 4.

We have also cross-correlated our source list with those of other ongoing ROSAT surveys, particularly those which have as their aim the discovery of clusters of galaxies (e.g., SHARC, Romer et al. 2000; CfA 160 deg<sup>2</sup>, Vikhlinin et al. 1998b). The information from these cross-correlations is given and appropriately referenced in Table 2.

## 2.3. **Optical Follow-up Program**

Once candidates for follow-up were selected according to the procedure laid out in § 2.2, we designed a program of optical imaging and spectroscopy, with a further selection step in between the imaging and spectroscopy. The goal of the optical follow-up program was to identify all clusters in the WARPS sample and determine their redshifts. The optical follow-up program used many different telescopes for imaging and spectroscopy. Our WWW page gives details of the observations for specific sources.

### 2.3.1. *Optical Imaging*

Images were obtained of cluster candidates, usually in the R band, which gives a good combination between high sensitivity, good chip cosmetics (i.e., no fringing), and sensitivity to galaxies at all but the highest redshifts where X-ray selected clusters are known (up to  $z \sim 0.9$ , where the Ca break passes out of the R band). These images were obtained at several different observatories (see the WWW page for details). Often an object was imaged more than once, either in R or I band, if the initial images revealed a still blank field, or

evidence of faint galaxies within the X-ray flux maximum region. Through this process, a total of 64 objects were found to coincide with an overdensity of galaxies and thus classified as cluster candidates.

### 2.3.2. Optical Spectroscopy

The next step in our optical follow-up was to observe spectroscopically the 64 objects identified as cluster candidates by the method described above. We also observed an additional 13 sources whose IDs are listed in Table 2. In Figure 1c, we show a histogram of the extent parameters  $f_{ext}$  of the sources selected for spectroscopy.

For each cluster candidate, we used X-ray/optical overlays to select galaxies for spectroscopy based not only upon their brightness but also their location relative to the X-ray centroid or peak(s). We attempted to associate galaxy groupings with each individual peak in the X-ray surface brightness distribution, not only to quantify the degree of possible point-source (*i.e.*, non-cluster) contamination, but also to account for superpositions of two truly extended sources. In obtaining spectra we typically used low dispersion gratings, and where possible multi-slit masks were designed in order to maximize our efficiency in identifying cluster members.

We identify an X-ray source as a cluster if (1) at least two galaxies (in the case of two or three spectra of good signal to noise) or at least three galaxies (in the case of four or more spectra) have very similar redshifts, and (2) if it can be reliably determined that the X-rays were not emitted by an AGN, star or other point source (some blends are present; see § 4.4). As a result of this program, 34 clusters were identified, 22 of which are above our flux limit of  $6.5 \times 10^{-14}$  erg cm $^{-2}$  s $^{-1}$ . In Table 4, we list information on each cluster; we will analyze the cluster population in more depth in § 4.

## 2.4. AGN in the WARPS-I sample

A significant number (22) of the objects we observed spectroscopically are AGN. These objects, along with those previously identified as AGN in other surveys (28 found via our NED and SIMBAD cross-correlations), are listed as such in Table 2. Several of these AGN are located in fields with significant galaxy overdensities, suggesting that those objects may reside in a group or cluster of galaxies. Rich environments are relatively common among AGN, particularly radio-loud AGN (*e.g.*, Ellingson et al. 1991). A small fraction of the X-ray emission in objects of this sort might originate in a hot intracluster medium (as found for

several 3CRR quasars and radio galaxies by Hardcastle & Worrall 1999); however, we believe this fraction is too small to constitute a significant source of error in our  $\log N$  -  $\log S$  or luminosity function.

### 3. Efficacy of VTP and Comparison with Other Surveys

WARPS is one of several X-ray surveys for clusters of galaxies based on archival ROSAT data. These surveys differ operationally in two main ways: (1) in the source detection algorithm, including the method by which sources are classified as extended; and (2) in the optical follow-up carried out, specifically the design of the imaging program.

As already mentioned, in WARPS we replaced the standard sliding box detection algorithm, which has difficulties detecting extended sources of low surface brightness, with the VTP algorithm (§ 2.1). VTP is one of several such algorithms currently in use for the detection of clusters in archival X-ray data. Three of the others are based on wavelet techniques (in particular those used by the RDCS, SHARC-Bright and CfA 160 deg<sup>2</sup> teams), while another is based on modifying the sliding box algorithm with smoothing and wavelet transforms (the SHARC-south survey, Collins et al. 1997). At least in theory, both VTP and wavelet techniques should be equally sensitive to surface brightness enhancements, regardless of their extent or morphology.

While the basic outlines of the optical follow-up program for each survey are similar, some important differences exist. Chief among these are the following. (1) WARPS is the only survey which performed optical imaging on sources which were not flagged as possibly extended by its detection algorithm (see § 2.3.1). (2) RDCS is the only survey that has included near-infrared imaging in its follow-up program. (3) SHARC-Bright is the only survey that used a completely automated 'friends-of-friends' analysis to screen for possibly blended X-ray sources. Each of these could conceivably have an impact on the completeness and content of the respective samples.

A comparison of the number counts as well as the results in overlapping fields is useful in judging the efficacy of each procedure, and the completeness of each sample. The efficacy of a detection algorithm in detecting extended sources can be judged in several ways. The first is to compare the number of sources that were extended by eye in a given field with the number of extended sources found by the detection algorithm. This is what might be called the "false negative" detection rate. For WARPS, such a visual inspection was done for every field as a part of the deblending process detailed in Paper I. These inspections were originally done as part of an effort to distinguish blends of two or more point sources from truly

extended X-ray sources, but they also have the side benefit of being able to find extended sources which may have been missed by VTP. This visual examination yielded only one more possibly extended source, listed multiply as WARPJ1414.9+1120, WARPJ1415.0+1119 and WARPJ1415.2+1119, compared to over 30 extended sources. It should be noted that this source *was* found by running VTP at the lowest of the three thresholds described in Paper I, but was removed by the deblending process that paper described, and manually returned to the catalog after our by-eye inspections. It is also not surprising that this source is extremely faint and in fact does not make our flux-limited sample (§ 4). This very low fraction of “lost” sources gives us considerable confidence in the reliability of VTP for detecting all extended and point sources up to our selected flux limit (for a discussion of the statistical significance of this flux limit see Paper I).

A second way to test the efficacy of our selection method, and in particular  $f_{ext}$ , described in § 2.1 and Paper I, is to look at the relationship between the fraction of truly extended X-ray sources (i.e., clusters, elliptical galaxies, etc.) and  $f_{ext}$ . In Figure 1d we show a histogram of the fraction of sources identified as clusters, as a function of  $f_{ext}$ . As can be seen, one of the clusters in our flux-limited sample has  $f_{ext} < 1.1$  (WARPJ2302.8+0843), and two more likely clusters with  $f_{ext} < 1$  fall below the limit (WARPJ1537.7+1201 and WARPJ1501.0–0824, which are in high-background fields). These clusters were identified only because our optical follow-up program included not only all possibly extended sources, but also sources flagged as not extended by VTP, that might be associated with visible galaxies or were blank fields. The cluster fraction increases markedly at higher values: 11% of sources with  $1.1 < f_{ext} < 1.2$  are clusters, but about 47% of sources with  $f_{ext} > 1.2$  are clusters. A similar fraction holds at higher extents. The fact that it never approaches unity attests to the fact that a significant number of X-ray blends are present. This pattern gives us further confidence in the efficacy of VTP as a method to detect extended sources.

It is not surprising that two of three clusters with  $f_{ext} < 1.1$  are among our faintest and most distant. Simulations by Evrard & Henry (1991) showed that cosmological  $(1+z)^{-4}$  surface brightness dimming can cause a cluster to appear as a point source at high  $z$ . Those authors predicted that ROSAT would begin to have trouble distinguishing extended X-ray emission in clusters from point-like sources, at redshifts  $z > 0.4$ . The results of this and other X-ray surveys for clusters of galaxies (Papers I, II; Romer et al. 2000; Collins et al. 1997; Rosati et al. 1998; Vikhlinin et al. 1998b) have shown that this prediction was too pessimistic, perhaps partly due to evolution of the spatial and/or spectral distribution of the ICM in clusters with redshift (which is predicted in hierarchical models of structure formation; see Bahcall & Cen 1992; Viana & Liddle 1996), or the presence of substructure and less centrally concentrated emission. However, at particularly high redshifts this effect should not be forgotten and may be a cause of incompleteness not only in our survey but in

all ROSAT-based surveys (see also the simulations by Adami et al. 2000).

The third and final way to test efficacy is to compare the overall number counts in WARPS with those of other surveys. If indeed all of the methods being employed are comparably effective in finding extended X-ray sources and hence clusters, we should find comparable log N - log S distributions. Rosati et al. (1998) have already addressed this issue regarding the comparison of WARPS-I with RDCS: despite the fact that RDCS has found a few clusters at  $z > 1$  (Rosati et al. 2000), the overall number counts are comparable. The situation is similar for the 160 deg<sup>2</sup> survey of Vikhlinin et al. (1998b), which has a log N - log S distribution similar to WARPS-I (Vikhlinin et al. 1998b, their Fig. 10). Moreover, since that survey has published its catalog we can cross-check the sources and IDs in the fields that are in common between the two. A total of 20 ROSAT fields are common to WARPS and 160 deg<sup>2</sup> survey, and the sources and IDs agree well (in particular the cluster IDs are in complete agreement in the overlapping regimes of flux and detector area, and the fluxes also agree well, with a mean ratio of VMF/WARPS=0.98 ± 0.26). The sources in common are noted in Table 3. Finally comparing the number counts of WARPS-I and SHARC-south (Collins et al. 1997; Burke et al. 1997) we see that the two curves are also comparable.

Some similar comparisons can also be made with the SHARC-Bright survey (Romer et al. 2000; Adami et al. 2000), which however have not published a log N - log S distribution. Unlike for all the other surveys, however, for SHARC-Bright we have reason to suspect serious inconsistencies. Comparing our field list with that of SHARC-Bright (Romer et al. 2000) we find 60 fields in common. WARPS finds all 6 of the clusters found by SHARC-Bright in those fields (down to the SHARC-Bright flux limit), as well as two not found by SHARC-Bright: WARPJ1552.2+2013 and WARPJ0238.0–5224. The overall number counts also do not agree: SHARC-Bright find 37 clusters with fluxes  $F_x \gtrsim 2.8 \times 10^{-13}$  erg cm<sup>-2</sup> s<sup>-1</sup> (as explained in Romer et al. 2000, this limit is approximate because they perform their limit calculation in counts, rather than flux), in a total area of 178.6 deg<sup>2</sup>. By comparison, our published log N - log S distribution (Paper II) predicts 57 ± 8 clusters within the SHARC-Bright survey - i.e., the number counts for SHARC-Bright are too low compared with the WARPS-I, SHARC-S, RDCS and CfA 160 deg<sup>2</sup> surveys, at the 2.5  $\sigma$  level.

A similar difference in number counts is found when comparing the extended source lists of the CfA 160 deg<sup>2</sup> and SHARC-Bright surveys, Romer et al. (2000, see their §7.5) note that SHARC-Bright finds only 13 of 21 CfA 160 deg<sup>2</sup> clusters that are both within the SHARC-Bright survey area and above the SHARC-Bright flux limit. This is consistent with the above comparison of the WARPS-I log N - log S with the total number of galaxies from SHARC-Bright. Of the 8 CfA 160 deg<sup>2</sup> clusters missed by SHARC-Bright, 7 did not meet the SHARC-Bright “filling factor” criterion (essentially an automated friends of friends analysis

intended to spot blends), while 1 did not meet their extent criterion. Thus a comparison to both our results and that of the CfA 160 deg<sup>2</sup> results suggests either serious incompleteness, or systematic miscalculation of cluster fluxes by SHARC-Bright.

Romer et al. (2000) have addressed this last point by comparing the fluxes for sources in common between SHARC-Bright and the CfA 160 deg<sup>2</sup>. They find that SHARC-Bright find systematically higher fluxes than the 160 deg<sup>2</sup> survey, with a mean ratio SHARC-B/VMF =  $1.18 \pm 0.26$ , and attribute the difference to assuming a fixed core radius of 250 kpc (when the Vikhlinin et al. 1998b core radius values are used the systematic difference disappears). We find a similar average ratio SHARC-B/WARPS =  $1.37 \pm 0.26$  but we are unable to test whether this would be removed by using the SHARC-Bright pipeline with our core radii.

If indeed SHARC-Bright do miscalculate their fluxes by 20-30% compared to other surveys, this would bring their overall number counts into agreement with those of WARPS-I and the CfA 160 deg<sup>2</sup>. However this still does not explain the failure of SHARC-Bright to find  $\sim 30 - 40\%$  of clusters which meet their flux limit. Romer et al. (2000) conclude in their paper that this “illustrates how differing selection criteria produce differing cluster samples and that detailed simulations are required to determine a survey’s selection function.” These were done in Adami et al. (2000), which simulated the selection function by placing cluster sources of various X-ray morphology randomly in real PSPC data. Interestingly, however, Adami et al. (2000) do not test explicitly the filling factor criterion which appears to have been responsible for SHARC-Bright missing fully 1/3 of the clusters within their survey area. What Adami et al. (2000) do instead is place simulated clusters randomly in real PSPC data, which does *implicitly* test the filling factor criterion, but they compile no statistics regarding *e.g.*, the nearness of the simulated cluster to other sources in each field. Thus despite the size of this correction (evidently 30-40%), the SHARC-Bright team does not test explicitly a major part of their selection function, making their results very hard to duplicate or verify independently. Thus their analysis contains many more uncertainties than other surveys

Because of the exhaustive nature of the WARPS optical follow-up program (§ 2.3), we can make one further comment. Unlike all the other surveys WARPS investigated thoroughly all possible cluster sources, even if the source was not extended according to the VTP algorithm. All other ROSAT based surveys did not image optically any sources that were not found to be extended by their source detection algorithm. The similarity of the WARPS, SHARC-south, RDCS and 160 deg<sup>2</sup> number counts, plus the fact that we only found one cluster in our complete sample among the sources we flagged as not extended, assures us that for our sample as well as the RDCS and CfA 160 deg<sup>2</sup> this effect is negligible overall, but may not be insignificant at the highest redshifts, although the size of the effect depends on the details of the algorithm used. However, the utility of this practice becomes clear in the

comparison with SHARC-Bright (above), since the careful evaluation of questionable sources and followup optical observations of those sources would have enabled them to identify the missing 30-40% of *bona fide*, X-ray bright clusters within their survey area and flux limits.

## 4. Clusters of Galaxies

### 4.1. The Cluster Catalog

In Table 4 we have listed all 22 members of the statistically complete WARPS-I cluster sample. Similarly, in Table 5 we list 13 additional clusters and 3 possible other clusters. Individual descriptions of all the sources in given in § 4.4. The columns in Table 4 and Table 5 are as follows:

1. The assigned cluster name.
2. The right ascension (hours, minutes, seconds) in J2000 coordinates, as extracted from the ROSAT data.
3. The declination (degrees, minutes, seconds) in J2000 coordinates, as extracted from the ROSAT data.
4. The extent parameter  $f_{ext}$  as discussed in § 2.1.
5. The hydrogen column density from Dickey & Lockman (1990) in units of  $10^{20} \text{ cm}^{-2}$ .
6. The unabsorbed source flux in units of  $10^{-13} \text{ ergs cm}^{-2} \text{ s}^{-1}$  in the 0.5–2.0 keV band as described in § 2.1. For some clusters this flux may include a component from contaminating sources (e.g., AGN). See § 4.4 for details for each cluster.
7. The rest-frame source luminosity in units of  $10^{44} \text{ ergs s}^{-1}$  in the 0.5–2.0 keV band derived in the same manner as the flux. Values of  $q_0 = 0.5$  and  $H_0 = 50 \text{ km s}^{-1} \text{ Mpc}^{-1}$  were assumed.
8. The core radius of the cluster in arcseconds. Note that this is very crude as it is based on ROSAT data which in most cases barely resolve the cluster.
9. The redshift of the cluster.
10. The number of galaxy redshifts used to derive the cluster redshift.

11. Flags. A “c” indicate that the cluster is contaminated or possibly contaminated by other sources. In Table 5, a “<” indicates that the cluster flux falls below the limit for inclusion in the statistically complete, flux-limited sample. An “?” indicates a possible cluster or group for which optical follow-up was not completed, usually because it was below the flux limit. An “8” indicates that the cluster was found in a field targeted at another cluster while an “b” indicates that this field was dropped due to high background. See the notes in § 4.4 for flagged sources.
12. Alternate names or notes. The same as for Table 2.

In Figure 3 we show the optical images we obtained of these clusters, with the X-ray emission contours overlaid. These images, as well as other information, are also available on our WWW site.

## 4.2. Radio Sources

In Table 6, we list the position, positional error, distance from the x-ray centroid, and flux of all radio sources within 2' of the X-ray centroid of each of these clusters, along with information regarding the possible nature of the radio sources (see also § 2.2.2). In each case we have checked to see whether some fraction of the X-ray emission could come from the radio source, and make comments to this effect in § 4.4.

## 4.3. The Statistically Complete WARPS-I Sample

We have selected from the sources identified as clusters a statistically complete, X-ray surface brightness limited sample of 22 clusters. This sample is somewhat different from the sample used to derive the  $\log N - \log S$  in Paper II. To make the WARPS-I sample consistent with that from WARPS-II, the PSPC field selection criteria for the statistical sample were made more restrictive (see § 2), and all the fields were reprocessed by VTP. The VTP algorithm was improved and refined between the WARPS-I and WARPS-II processing. This has changed the fluxes and extents slightly, by 5-10%, for some sources. A few clusters used in Paper II now fall below the flux limit (while others are now above it). However, these changes do not affect the conclusions of Paper II.

Figure 4 shows a histogram of the redshift distribution of the sample. As can be seen, the clusters in the WARPS-I sample range in redshift from  $z = 0.06 - 0.75$  (see also Table 4).

#### 4.4. Descriptions of Individual Clusters

Here we provide detailed information about clusters in both the statistical and supplemental samples. See Figure 3 for optical CCD images with X-ray emission contours overlaid. In this section, SHARC-B refers to the SHARC Bright Survey catalog (Romer et al. 2000), VMF to the CfA 160 deg<sup>2</sup> survey (Vikhlinin et al. 1998b), and RIXOS to the RIXOS survey catalog (Mason et al. 2000).

**WARPJ0022.0+0422** This extended X-ray source is associated with a cluster, GHO00190.5+0405 (no previous redshift), which was previously discovered by Gunn et al. (1986). An HRI observation of this field failed to detect the cluster, but it is near the edge of the HRI field-of-view. The northeastern X-ray component is identified with an AGN at  $z = 0.272$ , unrelated to the cluster. Aperture photometry on the PSPC image suggests that the quoted flux includes a  $\approx 25\%$  contribution from the AGN. This cluster is in a ROSAT field targeted at another cluster (GHO 0020+0407 at  $z=0.698$ ) and so is not part of the statistically complete sample.

**WARPJ0023.1+0421** This X-ray source originates in a poor cluster of galaxies at  $z = 0.453$ . An HRI observation of this field shows a marginal detection of an extended source. All the 7 galaxies for which spectra were obtained, including the 3 cluster members, show evidence of narrow emission lines. The brightest cluster member, offset from the X-ray peak, has O II emission and strong H $\delta$  absorption, indicative of recent star formation activity. The cluster galaxy at the X-ray peak has strong O II and weaker H $\beta$  and O III emission, indicative of a cooling flow or LINER-type spectrum rather than a Seyfert 2. This cluster is in a ROSAT field targeted at another cluster (GHO 0020+0407 at  $z=0.698$ ) and so is not part of the statistically complete sample.

**WARPJ0111.6–3811** The galaxies associated with this X-ray source appear to fall into two regions: a northern cluster at  $z = 0.121$  ( $n_z = 3$ ) and a south western one at  $z = 0.132$  ( $n_z = 4$ ). The x-ray emission originates predominantly from the northern cluster (the southern cluster clearly falls well below our flux limit). The VTP flux estimate excludes the southern cluster and the bright point-like X-ray source to the southeast, which is identified with a QSO at  $z = 0.894$ .

**WARPJ0144.5+0212** This clearly extended X-ray source corresponds with the position of a poor cluster of galaxies at  $z = 0.165$ , revealed by the optical image (Figure 3). The extended nature of the X-ray emission and the position of the BCG coincident with the X-ray peak makes it clear that the majority of the X-ray emission comes from the cluster, but the presence of an 80 mJy radio source (Table 6) makes some

caution advisable. The radio source corresponds to one of the fainter galaxies very near the BCG, which may be a background radio galaxy or other AGN. However, we see no evidence for X-ray point-like emission at this position so the possible contribution from the radio source is small. A second, much fainter, radio source is located in this cluster’s outskirts. The quoted flux includes both northern and southern X-ray components.

**WARPJ0206.3+1511** Our redshift is from two galaxies but agrees with the redshift in the RIXOS catalog and the estimate in the VMF catalog. The quoted X-ray flux may include a small contribution from a bright star to the east of the cluster.

**WARPJ0210.2–3932** The cluster was discovered during the reprocessing and corresponds to VMF 24. VMF estimate a photometric redshift of  $z = 0.19$ . Since it is well below our flux limit, no spectroscopic follow-up was done.

**WARPJ0210.4–3929** Our redshift for this cluster ( $z = 0.273$ ) is tentative, being based on low signal to noise observations at the CTIO 1.5m and at the AAT in service time. In both instances, spectra were taken of the two galaxies near the X-ray centroid. Those spectra show a continuum break at about 5000 Å in both galaxies and probable CaII at 4994/5059 Å and H $\beta$  at 6203 Å in the brighter galaxy only. This cluster is also in the VMF catalog, who estimate a photometric redshift of  $z = 0.27$  with a range of 0.20-0.30. Further spectroscopic observations are required to confirm the redshift of this cluster.

**WARPJ0216.5–1747** This clearly extended X-ray source corresponds to the position of the optical cluster shown in Figure 3. Also in the X-ray error circle (and near X-ray peaks) are 2 M stars. A 7.2 mJy radio source (Table 6) is about 100'' north of the X-ray centroid (and well outside the X-ray emission contours) which is associated with a foreground 14th magnitude galaxy. The X-ray image shows no sign of point source contamination, and we estimate that <30% of the PSPC flux is from the M stars, consistent with the  $\alpha_{ox}$  of M stars in Stocke et al. (1991).

**WARPJ0228.1–1005** This clearly extended X-ray source is associated with a cluster which is dominated by two bright galaxies that overlap on the sky. We only have a redshift ( $z = 0.149$ ) for one of them. The spectrum of the other galaxy contains only very weak absorption lines, and may possibly be a BL Lac object. It is also a faint radio source (7 mJy, Table 6). The HRI image confirms the cluster to be an extended X-ray source and also shows an unrelated point X-ray source  $\approx 1'$  to the northwest of the cluster. The quoted PSPC flux includes a  $\approx 10\%$  contribution from this source.

**WARPJ0234.2–0356** This distant ( $z = 0.447$ ) cluster falls just below the flux limit of our sample at  $6.4 \times 10^{-14}$  ergs cm $^{-2}$  s $^{-1}$ . The X-ray contours and the galaxy velocities (although from only 5 cluster members) suggest that the cluster has two components. The BCG of the northern component has narrow O II, O III and H $\alpha$  emission lines, as well as strong H $\delta$  absorption, perhaps indicating recent star-formation activity. It may be interacting with a nearby galaxy.

**WARPJ0238.0–5224** This massively extended X-ray source corresponds with the cluster Abell 3038. This source is also in the VMF and SHARC-B catalogs, but only in one of two fields within which the cluster is actually found (see § 3. We used the redshift from (Nesci & Altamore 1990), which has been confirmed by SHARC. An HRI image confirms the lack of point-source contamination.

**WARPJ0250.0+1908** We have only poor quality optical images of this source and two redshifts. However, this source is also in the SHARC-B catalog, who list a similar redshift ( $z = 0.12$ ). The northern X-ray source, visible on the contours, is excluded from the quoted X-ray flux.

**WARPJ0255.3+0004** This marginally extended source was imaged with the WIYN 3.5m revealing a possible distant group or poor cluster, but as it was below the flux limit, no further follow-up was done.

**WARPJ0348.1–1201** This extended X-ray source emanates from the unrelaxed  $z = 0.4876$  cluster shown in the optical image. The brightest galaxies in this cluster fall along a southeast to northwest line. One of these is a 34 mJy radio source (Table 6), but no X-ray point-like emission is evident near the position of this radio source.

**WARPJ0951.7–0128** This clearly extended X-ray source is associated with a  $z = 0.567$  cluster of galaxies. Our redshift agrees very well with the photometric estimate published in the VMF catalog. Our cross-correlations with the NVSS and FIRST revealed a 6.2 mJy radio source near the X-ray centroid (Table 6). The optical counterpart to this radio source is a 20th magnitude galaxy, likely a cluster member. We see some evidence for unresolved X-ray emission near this position, so some of the X-ray emission may originate from the radio source. We have only one firm redshift for this cluster and one other probable similar redshift.

**WARPJ1113.0–2615** The galaxies close to the brightest galaxy in this distant ( $z = 0.725$ ) cluster show morphological evidence for interactions, and perhaps a gravitationally lensed arc. The X-ray source is clearly extended but low surface brightness and is very close to the flux limit for our statistically complete sample. Based on visual inspection

of our deblending results, we have used the count rate at threshold 3 (rather than 4) for this object.

**WARPJ1406.2+2830** We obtained only a poor image and one low quality redshift of  $z = 0.552$  for the BCG of this source. This source is also listed in the CRSS survey (Boyle, Wilkes, & Elvis 1997), but as a galaxy only; the CRSS give a redshift of 0.546, also based on a low quality spectrum. VMF list this source with the CRSS redshift, but also identify the source as a cluster. We observed this cluster with the HRI in 1996, with exposure time 19900 seconds, but the HRI failed to detect extended emission from the cluster or any point source contamination. Given the lower sensitivity of the HRI compared to the PSPC to low surface brightness X-ray emission, this result supports supports the assertion that this X-ray source is indeed extended.

**WARPJ1406.9+2834** An HRI image shows an extended source at the position of the cluster plus a point X-ray source  $90''$  east of the cluster center. The flux quoted includes the flux from the point source, but analysis of the HRI image indicates that the point-source flux is at most 25% of the cluster flux. This source is also in the VMF and SHARC catalogs.

**WARPJ1407.6+3415** This extended X-ray source falls somewhat below our statistically complete sample's flux limit. We have one low quality redshift at  $z = 0.577$  and another at  $z = 0.3793$ , which contains narrow emission lines (O II equivalent width is  $20\text{\AA}$ ). This may be a cluster contaminated by a foreground star-forming galaxy or LINER. No further follow-up was done.

**WARPJ1415.1+3612** This distant cluster contains a 5.4 mJy radio source near the center of the X-ray contours possibly associated with the cluster BCG. The X-ray morphology indicates possible point-source contamination. We have obtained optical spectroscopy of this cluster with Keck but the data are noisy and we have been unable to extract a redshift.

**WARPJ1415.3+2308** This poor cluster, the lowest redshift cluster in the sample at  $z = 0.064$ , is dominated by two bright, probably interacting, galaxies. One of these galaxies has strong narrow H $\alpha$  emission and may contain a low luminosity AGN. An 8.7 mJy radio source is also present in the cluster center and coincides with one of the bright central galaxies. The X-ray morphology, although from a low signal-to-noise image, may indicate some point-source contamination from within the cluster, as well as extended emission. This cluster has been omitted from the statistically complete sample since it is in a ROSAT field targeted at another galaxy cluster.

**WARPJ1416.4+2315** This extended X-ray source originates in a  $z = 0.135$  cluster of galaxies visible on both the sky survey plate and the deeper image. A 4.1 mJy radio source (Table 6) appears to be associated with the BCG. Two of the three galaxies with redshifts (but not the BCG) show strong narrow H $\alpha$  emission, and one may be associated with weak X-ray emission. The X-ray flux from a QSO (HS1414+2330) behind the cluster also contributes to the quoted flux at about the 25% level according to the WGACAT, (White et al. 1995), but both of these sources are weak contaminants compared to the bright extended cluster emission. This a candidate for being a ‘fossil’ group or cluster of galaxies. This cluster has been omitted from the statistically complete sample since it is in a field targeted at another galaxy cluster.

**WARPJ1418.5+2511** This massively extended, luminous ( $L_{X,bol} \sim 10^{45}$  erg s $^{-1}$ ) X-ray source originates in a  $z = 0.29$  cluster of galaxies which can be seen both on the sky survey plate and the KPNO image. Our cross-correlation with the NVSS reveals a 38.9 mJy radio source 65'' from the X-ray centroid (Table 6), which is associated with a likely cluster member. We see no X-ray enhancement at the position of the radio source, so it is unlikely to contribute a major fraction of the X-ray emission. The FIRST image reveals that this radio source may have a wide-angle-tail morphology, which is not at all atypical of cluster radio galaxies (e.g., Ledlow & Owen 1995), although such sources are more commonly found in cluster cores. The Butcher-Oemler properties of this cluster have been studied by Fairley et al. (2001). The cluster has been previously discussed by Stocke et al. (1983) and other authors, as part of the Einstein Observatory Medium Sensitivity Survey (MSS, but note that this source is not in the later EMSS), and by Nandra et al. (1993) (it is only  $\approx 8'$  from the bright Seyfert 1 galaxy NGC 5548).

**WARPJ1501.0–0824** This is one of two point-like X-ray sources identified by our optical imaging program as a likely cluster of galaxies. We have not obtained optical spectroscopy since its X-ray flux is below the limit for our statistically complete sample. Aperture photometry of the BCG yields  $R = 19.54 \pm 0.3$ , which corresponds to a redshift estimate of  $z = 0.51 \pm 0.07$  using the photometric estimation method of Vikhlinin et al. (1998b). Our cross-correlation with the NVSS (Table 6) finds a resolved radio source 23'' from the X-ray source, which appears to be associated with a likely cluster galaxy. This indicates possible emission from an AGN; however, the radio position is well outside the X-ray position’s error circle, and in addition the position of the radio source is well away from the optical center of the cluster. The field was later removed from consideration in the statistically complete sample due to its high background.

**WARPJ1515.5+4346** This cluster was included as part of a larger extremely diffuse

source which was later resolved into three groupings. The northern clump (now WARPJ1515.7+4352) appears point-like and spectroscopy reveals a broad-lined AGN at  $z = 0.524$ . The southern clump is WARPJ1515.5+4346 at  $z = 0.135$  ( $n_z = 3$ ) but is just outside the  $15'$  radius from the ROSAT field center. The identification of the central source is uncertain. It may be a cluster with a redshift  $z = 0.136$  ( $n_z = 1$ ) or  $z = 0.237$  ( $n_z = 2$ ). By itself, the central source is below our count rate cutoff. Even if it is associated with WARPJ1515.5+4346, the centroid of the emission is still outside of the  $15'$  radius. Therefore, the cluster is not part of the statistically complete sample. This source corresponds to VMF 169, which has a listed position about  $4'$  north, suggesting that the VMF source includes more of the diffuse emission.

**WARPJ1517.9+3127** This distant ( $z = 0.744$ ,  $n_z = 2$ ), but luminous, cluster is just below our completeness threshold. In later reprocessing with an updated VTP it failed to even make the count rate cutoff. Therefore, it is not part of the statistically complete sample.

**WARPJ1537.7+1201** This X-ray source is associated with a group or poor cluster at  $z = 0.136$ . It has two X-ray emission components, which appear to be centered around the positions of the two brightest galaxies. This source was decomposed into two components and was manually reinserted following inspection of the X-ray photon distribution for the field. The source is in a ROSAT field with high background and so the cluster has been excluded from our statistically complete sample.

**WARPJ1552.2+2013** One of the member galaxies, located at a minor peak in the X-ray surface brightness, has narrow, and possibly broad,  $H\alpha$  emission. However, any contamination to the X-ray luminosity is at a small level. This system is a candidate ‘fossil’ group or poor cluster.

**WARPJ2038.4–0125** This extended X-ray source originates in one of the most distant ( $z = 0.679$ ) clusters of galaxies in the WARPS-I sample. Two radio sources are located in the field which may be associated with cluster galaxies (Table 6), but these are both well away from the X-ray emission contours.

**WARPJ2108.6–0507** This extended X-ray source is associated with a  $z = 0.222$  cluster which can be seen on both the sky survey plate and image. A faint (3.7 mJy; Table 6) radio source is located near the X-ray centroid, which does not appear to be associated with any of the brighter cluster galaxies as it is in a blank field according to our image. The X-ray morphology is compact; there may be a cooling flow or point-source contamination, although none of the optical spectra for three objects in the cluster core suggest that they are the counterparts.

**WARPJ2108.7–0516** This extended X-ray source is associated with a  $z = 0.317$  cluster of galaxies. A 9.6 mJy radio source (Table 6) located  $41''$  from the X-ray centroid, which does not correspond to the optical position of any galaxy visible on the CFHT image. We have 10 spectroscopically confirmed galaxy members. The cluster has at least two components, both in X-ray morphology and galaxy velocities. The x-ray source to the east is included in the quoted flux, but whether it is related to the cluster is not clear.

**WARPJ2146.0+0423** This massively extended X-ray source is associated with a  $z = 0.5324$  cluster of galaxies. Our cross-correlation with the NVSS (Table 6) reveals an unresolved radio source  $30''$  from the X-ray centroid. A likely cluster member is within the radio error circle, but the overlay of the optical and X-ray images does not indicate any enhancement of the X-ray emission near its position. The source extent and lack of point source contamination is confirmed by an HRI observation. This cluster is also in the Gunn et al. (1986) (GHO) sample. Oke (private communication) confirms the cluster redshift as  $z = 0.53$  (from 2 redshifts) and also finds two (emission line) galaxies at  $z=0.40$ , suggesting a superposed foreground cluster may exist. The Butcher-Oemler properties of this cluster have been studied by Fairley et al. (2001), who also find evidence for a foreground group. We have assumed all the X-ray flux originates in the  $z = 0.532$  system, since the X-ray emission is centered on the BCG of this system. A small fraction of the quoted X-ray flux may arise in the bright nearby elliptical galaxy visible in the overlay.

**WARPJ2239.4–0547, WARPJ2239.6–0543** These two sources were found to be associated with the cluster Abell 2465. The PSPC image shows two clearly extended X-ray sources, each centered on a well-defined cluster core. We have obtained optical spectroscopy of objects in both clusters, which confirms them to be at slightly different redshifts ( $z = 0.2419$  versus  $z = 0.2427$  for six galaxies apiece). We believe that these clusters may be in the process of merging. The brightest galaxy of WARPJ2239.6-0543 is also an 8.4 mJy radio source. However, the morphology in an HRI image does not reveal any point source emission, and none of the optical spectra of galaxies in the cluster core show emission lines.

**WARPJ2239.5–0600** This X-ray source is associated with a compact group at  $z = 0.174$ , and it falls just below the threshold for inclusion in our statistically complete sample at a flux of  $6.30 \times 10^{-14}$  ergs  $\text{cm}^{-2}$   $\text{s}^{-1}$ .

**WARPJ2302.8+0843** Keck imaging and spectroscopy of this distant cluster ( $z = 0.722, n_z = 1$ ) indicate that it may be contaminated by a BL Lac. This is supported by the presence of a 25 mJy radio source very close to the cluster center. The level of contamination is impossible to tell from the low signal-to-noise PSPC image. A recent image of this

source with *Chandra* shows that the X-ray emission is entirely extended, however (we will report on this image in a future paper).

**WARPJ2319.5+1226** We have only a good redshift for the BCG of this poor cluster or group ( $z = 0.125$ ) and have chosen to use the RIXOS value of  $z=0.124$  ( $n_z = 3$ ).

**WARPJ2320.7+1659** This clearly extended X-ray source is associated with a  $z = 0.499$  cluster of galaxies and a  $z = 1.81$  QSO at the x-ray peak. Most of the flux may be from the QSO, but the level of contamination is impossible to tell from the low signal-to-noise PSPC image. However, since the total flux is just above our flux limit, any small contribution from the QSO would reduce the cluster flux to a level below the flux limit, so we have excluded this source from our statistically complete sample. Our cross-correlation with the NVSS (Table 6) also reveals a 2.8 mJy radio source  $41''$  from the X-ray centroid, but no obvious X-ray enhancement is visible at this position.

## 5. Discussion and Future Prospects

Here we have presented the identifications and cluster catalogs from the first phase of the WARPS project, an extensive survey of deep ROSAT pointings using a surface brightness sensitive algorithm. In doing so, we have also presented some comparisons of the results of WARPS-I to other cluster surveys, which help place the the various cluster detection algorithms and follow-up programs in perspective. As can be seen, the findings of WARPS are largely similar to those of other cluster surveys as regards the space density of X-ray emitting clusters.

The number of serendipitous X-ray surveys for clusters of galaxies now number more than a dozen. For example, the list of those based on ROSAT data includes BCS (Ebeling et al. 1998, 1997, 2000), WARPS (Papers I, II), RDCS (Rosati et al. 1998), SHARC-Bright (Romer et al. 2000), SHARC-south (Burke et al. 1997; Collins et al. 1997), CfA 160 deg<sup>2</sup> (Vikhlinin et al. 1998b), NEP (Gioia et al. 2001), NORAS (Böhringer et al. 2000), REFLEX (Boehringer et al. 2001), MACS (Ebeling et al. 2001c) and CIZA (Ebeling, Mullis, & Tully 2001). Each of these surveys use different selection criteria and/or X-ray source-detection algorithms, but largely similar optical follow-up programs. Meanwhile, several optical surveys have used moderate depth, large-area images of the sky combined with algorithms that measure overdensities of galaxies (e.g., PDCS, Lubin 1995; Postman et al. 1996; RCS, Gladders & Yee 2000). All of these surveys represent a fertile ground for constraining cosmological parameters as well as learning more about appropriate methods for finding massive clusters of galaxies and their attendant selection effects. However, precious few efforts (most notably

ROXS, Donahue et al. 2000) are underway to understand the relationship of the selection effects in optical and X-ray surveys.

Despite the different emphases inherent in each method, all of the new surveys show no evidence for evolution at all but the most X-ray luminous clusters of galaxies at redshifts up to  $z = 0.8$ . The X-ray luminosity-temperature relationship (Paper IV, Mushotzky & Scharf 1997) at  $z < 0.8$ , also shows no sign of evolution. Yet at  $z \sim 1$ , there are tantalizing hints of evolution in the cluster population. This evidence includes a preponderance of irregular X-ray morphologies, optical cluster galaxy distributions and colors (Paper III, Stanford et al. 2001, although see Paper V for a notable counter-example), as well as a suggestion that the space density of the most luminous ( $L_X > 5 \times 10^{44}$  erg s $^{-1}$ ) clusters decreases significantly at redshifts  $z > 0.5$  (Rosati et al. 1998; Vikhlinin et al. 1998a; although for a counterargument see Paper V). Taken together, these lines of evidence might suggest that the epoch of cluster formation is currently just out of reach of our current observational tools, which are limited to finding clusters at  $z < 1.25$  by the limitations inherent in observing in the optical (at  $z = 1.25$  the Ca break passes out of the I band), even though simulations (*e.g.*, Paper I) show an ability to detect X-ray luminous, extended sources at redshifts up to nearly  $z = 2$ .

This presents future X-ray surveys (*e.g.*, *Chandra* or XMM-Newton) with significant challenges, since one would expect them to contain large numbers of  $z > 1$  clusters. Indeed, as we pointed out in Papers III and V, WARPS is sensitive enough to include clusters of  $L_X \sim 10^{45}$  erg s $^{-1}$  out to redshifts of nearly 2. Even given the highly unclear (and very poorly explored) state of galaxy evolution at  $z \gtrsim 1$ , it is obvious from the current literature that, at  $z \sim 0.8$ , the space density and ICM characteristics of clusters of galaxies show little difference from those observed at lower redshifts. It is therefore imperative that future surveys for clusters of galaxies include near-infrared observations, which should increase their window of sensitivity for identifying cluster counterparts to X-ray sources out to  $z \sim 4.5$  (*i.e.*, when the H & K break passes out of the K band). Of the current X-ray surveys, only RDCS has included near-infrared observations in its follow-up program, and as a result, RDCS is the only X-ray selected sample of clusters to contain  $z > 1$  objects (Rosati et al. 1999, 2000), albeit only a handful (4 according to Rosati et al. 2000 and P. Rosati, private communication from an incomplete survey of about 80% of RDCS blank-field X-ray sources).

The now overwhelming evidence of little or no significant evolution in the space density of clusters at redshifts up to 0.8 is difficult to reconcile with  $\Omega_m = 1$  cold dark matter cosmologies, which predict significant evolution in the cluster LF at  $z \gtrsim 0.3$ . However, as Bode et al. (2001) show, a great deal of degeneracy remains in the predictions of hierarchical models of structure formation at  $z > 1$ , and coincidentally, this is where the fewest such X-ray selected clusters are known. It is at these highest redshifts that future X-ray and

other surveys for clusters (notably Sunyaev-Zel'dovich effect methods, see Xue & Wu 2001) will have to concentrate their efforts and where they will have the most impact.

E. S. P. acknowledges support from *Chandra* grant SAO1800627. H. E. acknowledges support from NASA LTSA grant NAG5-8253. C. A. S. acknowledges support from NASA LTSA grant NAG5-3257 (PI: M. Donahue). L. R. J. acknowledges the support of the U. S. National Research Council and the UK PPARC. We acknowledge interesting conversations with and emails from P. Rosati, C. Norman, M. Donahue, J. P. Henry, J. T. Stocke, R. Mushotzky, M. Henriksen, A. Evrard and B. Mathiesen.

The WARPS team acknowledges the long-term support of many different time allocation committees, including those at Kitt Peak National Observatory, Cerro Tololo Inter-American Observatory and the University of Hawaii, for the observations detailed in this paper. Part of the observations used in this paper were obtained at the MDM Observatory on Kitt Peak in Arizona. Some of the data presented herein were obtained at the W.M. Keck Observatory, which is operated as a scientific partnership among the California Institute of Technology, the University of California and the National Aeronautics and Space Administration. The Keck Observatory was made possible by the generous financial support of the W.M. Keck Foundation. This research has made use of data obtained through the High Energy Astrophysics Science Archive Research Center Online Service, provided by the NASA/Goddard Space Flight Center. This research has made use of the NASA/IPAC Extragalactic Database (NED) which is operated by the Jet Propulsion Laboratory, California Institute of Technology, under contract with the National Aeronautics and Space Administration. This research has also made use of the NRAO-VLA Sky Survey, which was carried out at the NRAO Very Large Array. NRAO is a facility of Associated Universities, Inc., and is a facility of the (USA) National Science Foundation. Finally, we wish to thank our referee, Dr. Luigi Guzzo, for helpful comments which improved considerably this paper.

## REFERENCES

Adami, C., Ulmer, M. P., Romer, A. K., Nichol, R. C., Holden, B. P., & Pildis, R. A. 2000, ApJS, 131, 391

Bahcall, N. A., & Cen, R. 1992, ApJ, 398, L81

Becker, R. H., White, R. L., & Helfand, D. J. 1995, ApJ, 450, 559

Bode, P., Bahcall, N. A., Ford, E. B., & Ostriker, J. P. 2001, ApJ, in press, astro-ph/0011376

Boehringer, H., et al. 2001, A&A, submitted, astro-ph/0012266

Böhringer, H., et al. 2000, ApJS, 129, 435

Boyle, B. J., Wilkes, B. J., & Elvis, M., 1997, MNRAS, 285, 511

Briel, U. G., & Pfeffermann, E. 1995, Proc. SPIE, 2518, 120

Burke, D. J., Collins, C. A., Sharples, R. M., Romer, A. K., Holden, B. P., & Nichol, R. C. 1997, ApJ, 488, L83

Carlberg, R. G., Morris, S. L., Yee, H. K. C., & Ellingson, E. 1997, ApJ, 479, L19

Collins, C. A., Burke, D. J., Romer, A. K., Sharples, R. M., & Nichol, R. C. 1997, ApJ, 479, L117

Condon, J. J., Cotton, W. D., Greisen, E. W., Yin, Q. F., Perley, R. A., Taylor, G. B., & Broderick, J. J. 1998, AJ, 115, 1693

Dickey, J. M., & Lockman, F. J. 1990, ARA&A, 28, 215

Donahue, M. E., Scharf, C., Mack, J., Lee, P., Postman, M., Dickinson, M., Rosati, P., & Stocke, J. 2000, in American Astronomical Society Meeting 197, #57.02, Vol. 197, 5702

Ebeling, H. 1993, Ph.D. thesis, Ludwig-Maximilians-Universität München

Ebeling, H., Edge, A. C., Böhringer, H., Allen, S. W., Crawford, C. S., Fabian, A. C., Voges, W., & Huchra, J. P. 1998, MNRAS, 301, 881

Ebeling, H., Edge, A. C., Fabian, A. C., Allen, S. W., Crawford, C. S., & Böhringer, H. 1997, ApJ, 479, L101

Ebeling, H., et al., 2000, MNRAS, 318, 333

Ebeling, H., Edge, A. C., & Henry, J. P. 2001c, ApJ, 553, 668

Ebeling, H., Jones, L. R., Fairley, B., Perlman, E., Scharf, C. A., & Horner, D. 2001a, ApJ, 548, L23 (Paper V)

Ebeling, H., Mullis, C. R., Tully, R. B., 2001, ApJ, submitted

Ebeling, H., et al. 2001b, ApJ, 534, 133 (Paper III)

Ebeling, H., & Wiedenmann, G. 1993, Phys. Rev. E, 47, 704

Edge, A. C., Stewart, G. C., Fabian, A. C., & Arnaud, K. A. 1990, MNRAS, 245, 559

Ellingson, E., Green, R. F., & Yee, H. K. C. 1991, ApJ, 378, 476

Evrard, A. E., & Henry, J. P. 1991, ApJ, 383, 95

Fairley, B. W., Jones, L. R., Scharf, C., Ebeling, H., Perlman, E., Horner, D., Wegner, G., & Malkan, M. 2000, MNRAS, 315, 669 (Paper IV)

Fairley, B., et al., 2001, in preparation

Frenk, C. S., White, S. D. M., Efstathiou, G., & Davis, M. 1990, ApJ, 351, 10

Gioia, I. M., Henry, J. P., Mullis, C. R., Voges, W., Briel, U. G., Böhringer, H., & Huchra, J. P., 2001, /apjl, in press, astro-ph/0102332

Gladders, M. D., & Yee, H. K. C., 2000, AJ, 120, 2184

Gunn, J. E., Hoessel, J. G., & Oke, J. B. 1986, ApJ, 306, 30

Hardcastle, M. J., & Worrall, D. M. 1999, MNRAS, 309, 969

Henry, J. P., Gioia, I. M., Maccacaro, T., Morris, S. L., Stocke, J. T., & Wolter, A. 1992, ApJ, 386, 408

Horner, D. J., Mushotzky, R. F., & Scharf, C. A. 1999, ApJ, 520, 78

Irwin, M., Maddox, S., & McMahon, R. 1994, Spectrum, 2, 14

Jones, C., & Forman, W. 1984, ApJ, 276, 38

Jones, L. R., Scharf, C., Ebeling, H., Perlman, E., Wegner, G., Malkan, M., & Horner, D. 1998, ApJ, 495, 100 (Paper II)

Kaiser, N. 1991, ApJ, 383, 104

Ledlow, M. J., & Owen, F. N. 1995, AJ, 109, 853

Lubin, L. M., 1995, Ph. D. thesis, Princeton University

Lucey, J. R. 1983, MNRAS, 204, 33

Luppino, G. A., & Gioia, I. M. 1995, ApJ, 445, L77

Mason, K. O., et al. 2000, MNRAS, 311, 456

Mullis, C. R. 2000, in Large Scale Structure in the X-ray Universe, Proceedings of the 20-22 September 1999 Workshop, Santorini, Greece, eds. Plionis, M. & Georgantopoulos, I., Atlantisciences, Paris, France, p.149, 149

Mushotzky, R. F., & Scharf, C. A. 1997, *ApJ*, 482, L13

Nandra, K., et al. 1993, *MNRAS*, 260, 504

Nesci, R., & Altamore, A., 1990, *A&A*, 234, 60

Nichol, R. C., Holden, B. P., Romer, A. K., Ulmer, M. P., Burke, D. J., & Collins, C. A. 1997, *ApJ*, 481, 644

Owen, F. N., & Ledlow, M. J. 1997, *ApJS*, 108, 41

Postman, M., Lubin, L. M., Gunn, J. E., Oke, J. B., Hoessel, J. G., Schneider, D. P., Christensen, J. A., 1996, *AJ*, 111, 615

Rector, T. A., Stocke, J. T., Perlman, E. S., & Gioia, I. M., 1999, *ApJ*, 516, 145.

Romer, A. K., et al. 2000, *ApJS*, 126, 209

Rosati, P., Borgani, S., della Ceca, R., Stanford, A., Eisenhardt, P., & Lidman, C. 2000, in Large Scale Structure in the X-ray Universe, Proceedings of the 20-22 September 1999 Workshop, Santorini, Greece, eds. Plionis, M. & Georgantopoulos, I., Atlantisciences, Paris, France, p.13, 13

Rosati, P., Della Ceca, R., Norman, C., & Giacconi, R. 1998, *ApJ*, 492, L21

Rosati, P., Stanford, S. A., Eisenhardt, P. R., Elston, R., Spinrad, H., Stern, D., & Dey, A. 1999, *AJ*, 118, 76

Scharf, C. A., Jones, L. R., Ebeling, H., Perlman, E., Malkan, M., & Wegner, G. 1997, *ApJ*, 477, 79 (Paper I)

Snowden, S. L., Plucinsky, P. P., Briel, U., Hasinger, G., & Pfeffermann, E. 1992, *ApJ*, 393, 819

Stanford, S. A., Holden, B., Rosati, P., Tozzi, P., Borgani, S., Eisenhardt, P. R., & Spinrad, H. 2001, *ApJ*, in press, astro-ph/0012250

Stocke, J. T., Liebert, J., Gioia, I. M., Maccacaro, T., Griffiths, R. E., Danziger, I. J., Kunth, D., & Lub, J. 1983, *ApJ*, 273, 458

Stocke, J. T., Morris, S. L., Gioia, I. M., Maccacaro, T., Schild, R., Wolter, A., Fleming, T. A., & Henry, J. P. 1991, *ApJS*, 76, 813

Stocke, J. T., Perlman, E. S., Gioia, I. M., & Harvanek, M. 1999, *AJ*, 117, 1967

Struble, M. F., & Rood, H. J. 1991, *ApJ*, 374, 395

Sutherland, W. 1988, *MNRAS*, 234, 159

van Haarlem, M. P., Frenk, C. S., & White, S. D. M., 1997, *MNRAS*, 287, 817

Viana, P. T. P., & Liddle, A. R. 1996, *MNRAS*, 281, 323

Vikhlinin, A., McNamara, B. R., Forman, W., Jones, C., Quintana, H., & Hornstrup, A. 1998, *ApJ*, 502, 558

Vikhlinin, A., McNamara, B. R., Forman, W., Jones, C., Quintana, H., & Hornstrup, A. 1998, *ApJ*, 498, L21

White, N. E., Giommi, P., & Angelini, L. 1995,  
<http://heasarc.gsfc.nasa.gov/wgacat/wgacat.html>

White, R. L., Becker, R. H., Helfand, D. J., & Gregg, M. D. 1997, *ApJ*, 475, 479

White, D. A., Jones, C., & Forman, W., 1997, *MNRAS*, 292, 419

Xue, Y., & Wu, X. 2001, *ApJ*, in press, astro-ph/0101529

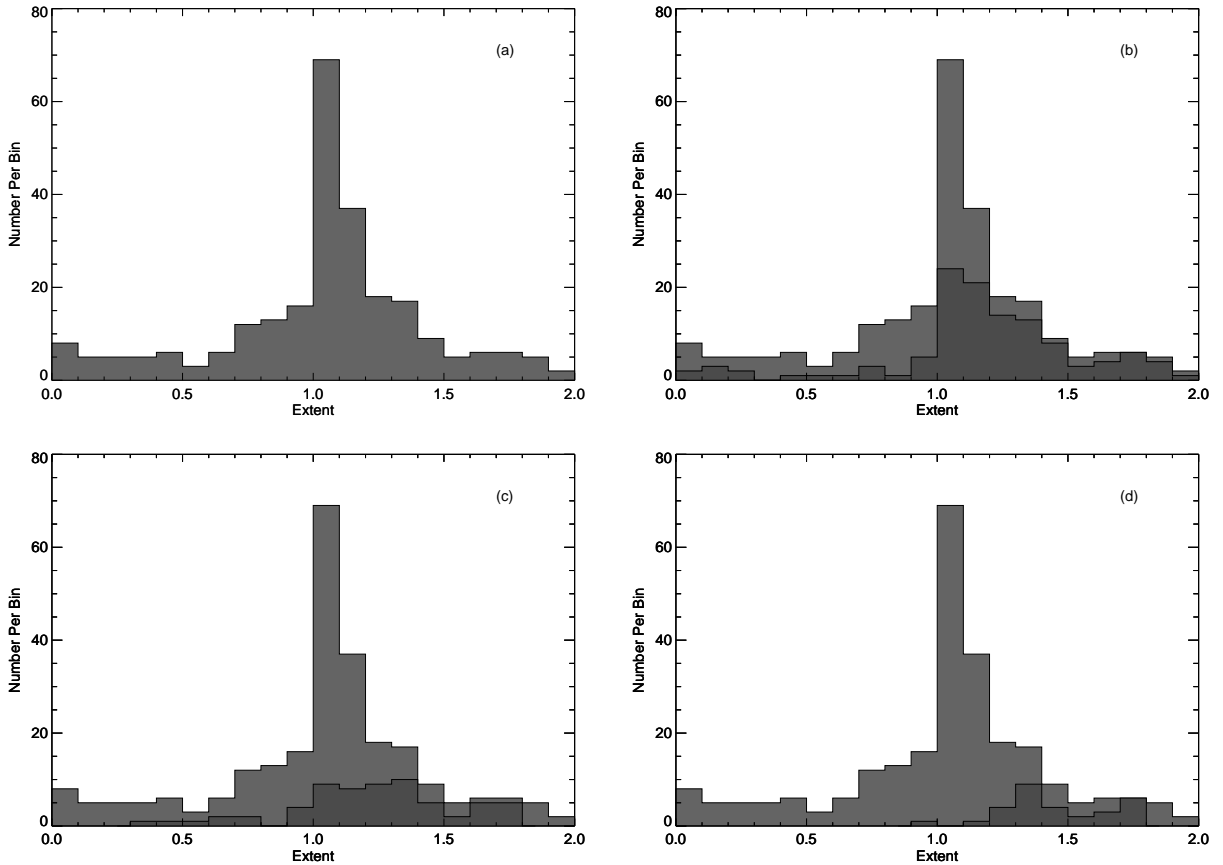


Fig. 1.— Histogram of the extent parameter for (a) all sources, (b) with sources selected for imaging, (c) with sources selected for spectroscopy, and (d) with confirmed clusters.

Fig. 2.— Overlays of the observed X-ray emission for the 60 extended or marginally extended sources on digitized plates from the POSS-I, UKST, or POSS-II surveys. Overlays for four additional X-ray sources which were found to be pointlike by VTP but were included as cluster candidates following our optical imaging program, are included at the end of the Figure. Each image is  $5' \times 5'$  with the standard orientation of north up and east to the left. The x-rays were smoothed with a  $45''$  Gaussian.

Fig. 3.— Overlays of the observed X-ray emission for each cluster on an optical (R-band) CCD image. Each image is 1.5 Mpc across at the cluster redshift (or  $5'$  if the redshift is unknown) with axes labelled in arc seconds from the VTP centroid with the standard orientation of north up and east to the left. The x-rays were smoothed with a  $45''$  Gaussian. Radio sources are labelled R1, R2, etc. as in Table 6 and are marked with a circle the size of the positional error given in the Table (which may be too small to see). Other sources (such as M stars) are also marked and labelled accordingly.

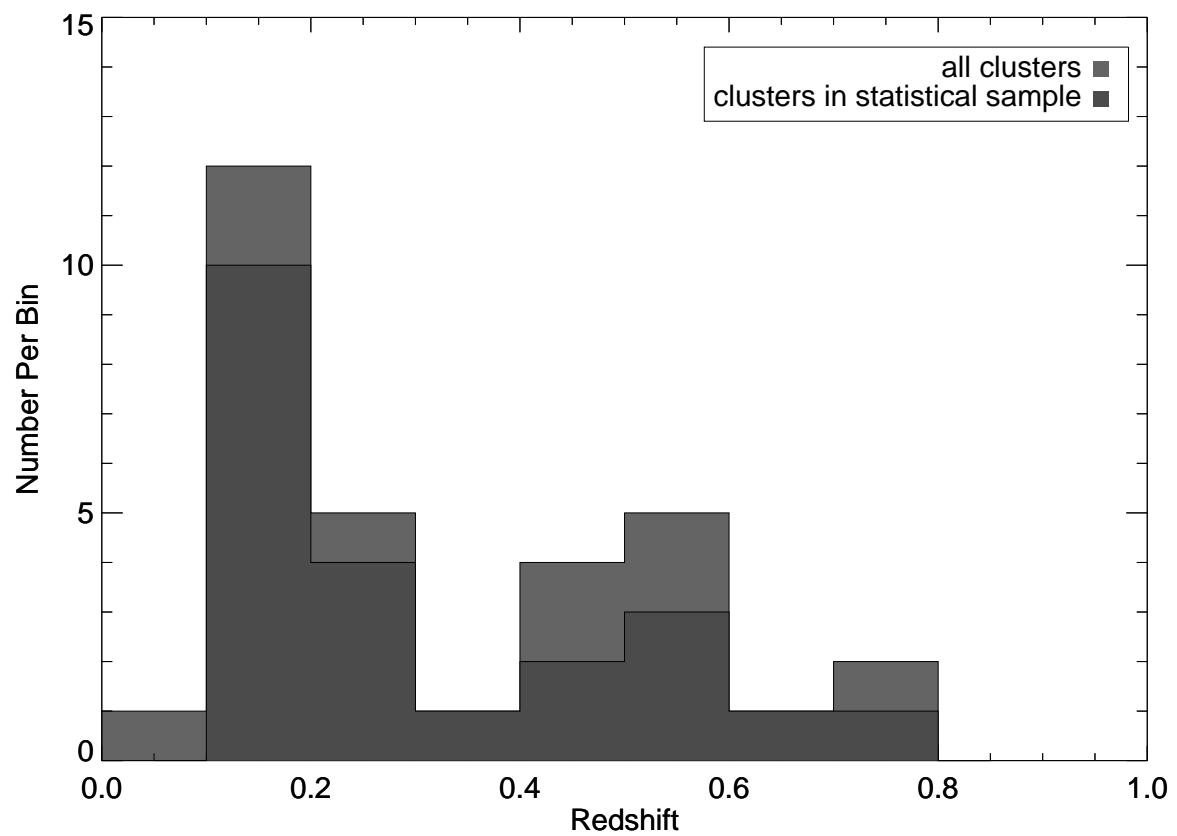


Fig. 4.— Redshift distribution of the cluster sample.

Table 1. ROSAT PSPC pointings used in WARPS

| Sequence ID | Expo [sec.] | $\alpha$ (J2000) | $\delta$ (J2000) | Target Name      |
|-------------|-------------|------------------|------------------|------------------|
| rp150071n00 | 17912       | 14 17 59.9       | +5 08 23.9       | NGC 5548         |
| rp200125n00 | 8614        | 16 55 33.6       | -08 23 24.1      | LHS429           |
| rp200474n00 | 9372        | 23 18 45.5       | +2 36 00.1       | KUV 2316+123     |
| rp200905n00 | 10327       | 15 13 33.5       | +8 34 11.8       | SS BOOTIS        |
| rp200965n00 | 10328       | 15 14 47.9       | +4 01 47.8       | PG1513+442       |
| rp201007n00 | 18199       | 21 09 19.1       | -13 14 24.1      | LHS 65           |
| rp201018n00 | 19015       | 15 18 11.9       | +1 39 00.1       | U CRB            |
| rp201019n00 | 10639       | 11 13 11.9       | -26 28 12.0      | TT HYA           |
| rp201037n00 | 15533       | 13 56 09.5       | +5 55 12.0       | ZZ BOO           |
| rp201045n00 | 28336       | 00 39 19.2       | +0 51 35.9       | S AND            |
| rp201070n00 | 8301        | 13 29 47.9       | +1 06 00.0       | HD117362         |
| rp201471n00 | 8373        | 13 11 52.7       | +7 52 48.1       | HD 114710        |
| rp201505n00 | 28004       | 18 42 38.3       | +5 32 24.0       | HD173524         |
| rp300003n00 | 24464       | 02 06 52.7       | +5 17 59.9       | TT ARIETIS       |
| rp300021n00 | 24506       | 16 05 45.6       | +5 51 35.9       | MS1603.6+2600    |
| rp300028n00 | 27116       | 13 48 55.2       | +7 57 35.8       | PG1346+082       |
| rp300043n00 | 14804       | 01 41 00.0       | -67 53 24.1      | BL HYI           |
| rp300079n00 | 49502       | 03 37 55.2       | -25 20 59.9      | EXO 033319-2554. |
| rp300180n00 | 45541       | 17 17 07.2       | +3 08 23.9       | NGC 6341         |
| rp300218n00 | 20662       | 20 38 14.4       | -01 21 00.0      | AE AQR           |
| rp300220n00 | 15603       | 23 16 02.3       | -05 27 00.0      | RX J2316.1-0527  |
| rp300389n00 | 36716       | 21 07 55.1       | -05 16 12.1      | RE2107-05        |
| rp400116n00 | 8303        | 12 59 59.9       | +2 40 11.9       | PSR 1257+12      |
| rp400293n00 | 20080       | 22 54 19.1       | +9 03 36.1       | GRB 910814       |
| rp400322n00 | 12424       | 00 19 50.4       | +1 56 59.9       | RX J0019.8+2156  |
| rp600119n00 | 11993       | 15 06 31.2       | +5 46 12.0       | NGC 5866         |
| rp600164n00 | 16752       | 12 58 59.9       | +4 51 36.0       | NGC 4861         |
| rp600439n00 | 11233       | 23 20 31.1       | +7 13 48.0       | III ZW 102       |
| rp600448n00 | 12808       | 14 34 52.8       | +8 40 48.0       | MARK 474/NGC 568 |
| rp600462n00 | 14242       | 14 15 33.5       | +6 13 47.9       | NGC 5529         |
| rp700006n00 | 12146       | 21 14 52.8       | +6 07 48.0       | PG2112+059       |
| rp700026n00 | 11197       | 04 22 14.3       | -38 45 00.1      | Q0420-388        |
| rp700027a01 | 17554       | 02 09 28.7       | -39 30 35.9      | Q0207-398        |
| rp700061n00 | 25728       | 14 06 57.6       | +8 27 00.0       | 1404+286         |
| rp700096n00 | 8038        | 15 59 09.6       | +5 01 47.3       | MKN493           |
| rp700101n00 | 24337       | 00 08 19.1       | +0 41 23.9       | MKN335           |
| rp700108n00 | 13683       | 01 43 57.6       | +2 21 00.1       | MKN573           |
| rp700114n00 | 9451        | 02 28 38.4       | -10 10 48.1      | 0226-1024        |
| rp700117n00 | 22456       | 14 06 43.2       | +4 11 23.6       | 3CR294           |
| rp700122n00 | 27863       | 14 15 45.6       | +1 29 42.0       | Q1413+1143       |
| rp700331n00 | 23437       | 00 48 45.6       | +1 57 35.8       | MKN 348          |
| rp700350n00 | 10028       | 02 35 07.1       | -04 01 48.0      | 0232-042         |
| rp700377n00 | 10718       | 00 46 14.4       | +1 04 11.8       | Q0043+0048       |
| rp700423n00 | 18562       | 23 03 14.4       | +8 52 12.1       | NGC 7469         |
| rp700432n00 | 13860       | 02 07 50.3       | +2 43 12.1       | NAB 0205+024     |
| rp700527n00 | 8898        | 14 19 04.7       | -13 10 48.1      | PG 1416-129      |
| rp700794n00 | 10830       | 01 11 28.8       | -38 04 48.0      | NGC 424          |
| rp700796n00 | 9004        | 13 10 57.5       | +7 03 36.0       | NGC 5005         |
| rp700797n00 | 9516        | 13 25 43.2       | -29 49 47.9      | NGC 5135         |

Table 1—Continued

| Sequence ID | Expo [sec.] | $\alpha$ (J2000) | $\delta$ (J2000) | Target Name      |
|-------------|-------------|------------------|------------------|------------------|
| rp700908n00 | 9043        | 09 52 19.1       | -01 36 35.9      | MKN 1239         |
| rp700920n00 | 12675       | 02 49 19.1       | +9 17 59.8       | MKN372           |
| rp700976n00 | 11171       | 01 24 45.6       | +9 18 35.8       | MS0122.1+0903    |
| rp700977n00 | 13951       | 02 08 38.3       | +5 23 24.1       | MS0205.7+3509    |
| rp701000a01 | 27821       | 13 43 43.1       | -00 14 59.8      | BJS864           |
| rp701018n00 | 11342       | 22 23 45.6       | -02 13 12.1      | 3C445            |
| rp701191n00 | 10395       | 22 12 59.9       | -17 10 12.1      | RX J2213.0-1710  |
| rp701205n00 | 14428       | 23 43 31.2       | -14 55 12.1      | MS2340.9-1511    |
| rp701206n00 | 9431        | 22 39 52.8       | -05 52 11.9      | BR 2237-06       |
| rp701213n00 | 14664       | 15 52 09.5       | +0 05 59.9       | 3C326            |
| rp701250n00 | 18765       | 23 04 43.1       | -08 41 23.4      | MCG-2-58-22      |
| rp701356n00 | 23554       | 02 37 12.0       | -52 15 36.0      | ESO198-G24/ WWHO |
| rp701373n00 | 15427       | 15 49 50.4       | +1 25 48.1       | 3C 324           |
| rp701403n00 | 11855       | 02 55 11.9       | +0 10 48.0       | NGC 1144         |
| rp701405n00 | 13356       | 15 26 07.2       | +1 40 11.8       | NGC 5929         |
| rp701411n00 | 22955       | 15 34 55.2       | +3 29 24.1       | ARP220           |
| rp701420n00 | 9940        | 21 58 07.2       | -15 01 11.9      | 2155-15          |
| rp800003n00 | 28248       | 15 58 55.2       | +3 23 23.8       | GC1556+335       |
| rp800150a01 | 12778       | 21 46 33.6       | +4 13 47.9       | 21 HOUR FIELD    |
| rp800401a01 | 11811       | 14 15 57.5       | +3 07 11.9       | 4C23.37          |
| rp800471n00 | 10639       | 04 30 45.6       | +0 24 36.1       | NGC 1588         |
| rp800483n00 | 26671       | 00 22 52.7       | +4 24 35.5       | CL0020           |
| rp900017n00 | 25815       | 04 40 55.1       | -16 30 36.1      | EDS - PSPC       |
| rp900242n00 | 11620       | 04 14 16.8       | -12 44 24.0      | NGC 1535         |
| rp900246n00 | 9152        | 04 11 40.7       | -17 28 48.1      | ERID1            |
| rp900325n00 | 10322       | 13 17 43.1       | +4 54 00.0       | G107+71          |
| rp900337n00 | 15618       | 22 25 48.0       | -04 57 00.0      | 2223-052         |
| rp900339n00 | 22143       | 22 53 57.5       | +6 08 59.9       | 2251+158         |
| rp900345n00 | 9346        | 21 27 55.2       | +2 58 12.0       | G064-26          |
| rp900352n00 | 10383       | 02 17 19.1       | -17 45 35.9      | G192-67          |
| rp900492n00 | 9609        | 03 48 23.9       | -12 10 11.9      | ERID4            |

Table 2. WARPS-I Source Catalog

| Name<br>(1)      | ROSAT<br>Field<br>(2) | $\alpha$<br>(J2000)<br>(3) | $\delta$<br>(J2000)<br>(4) | $cr_{raw}$<br>[ $10^{-3}$ ]<br>(5) | $cr_{corr}$<br>[ $10^{-3}$ ]<br>(6) | $n_H$<br>[ $10^{20}$ ]<br>(7) | Flux<br>[ $10^{-13}$ ]<br>(8) | Extent<br>(9) | Im<br>(10) | Sp<br>(11) | Id<br>(12) | Redshift/<br>Sp. Type<br>(13) | Other Name/<br>Notes<br>(14)    |
|------------------|-----------------------|----------------------------|----------------------------|------------------------------------|-------------------------------------|-------------------------------|-------------------------------|---------------|------------|------------|------------|-------------------------------|---------------------------------|
| WARPJ0008.4+2034 | rp700101n00           | 00 08 26.7                 | +20 34 31                  | 13.89                              | 15.93                               | 3.95                          | 2.07                          | 1.07          | ...        | ...        | qso        | 0.389                         | CRSS J0008.4+2034               |
| WARPJ0008.8+2050 | rp700101n00           | 00 08 53.9                 | +20 50 28                  | 52.15                              | 55.86                               | 3.93                          | 7.27                          | 0.82          | ...        | ...        | star       | M(e)                          | CRSS J0008.9+2050               |
| WARPJ0020.7+2205 | rp400322n00           | 00 20 43.3                 | +22 05 36                  | 6.14                               | 11.65                               | 4.14                          | 1.52                          | 1.81          | R          | Y          | ...        | ...                           |                                 |
| WARPJ0038.2+3053 | rp201045n00           | 00 38 12.4                 | +30 53 28                  | 8.70                               | 9.70                                | 5.6                           | 1.32                          | 0.41          | ...        | Y          | gal        | 0.018                         | UGC 00381                       |
| WARPJ0040.2+3054 | rp201045n00           | 00 40 12.1                 | +30 54 31                  | 10.43                              | 11.54                               | 5.6                           | 1.57                          | 0.98          | ...        | Y          | BLEND      | ...                           | Sy1/QSO+NELG+Galaxy             |
| WARPJ0045.2+0107 | rp700377n00           | 00 45 16.8                 | +01 07 03                  | 6.06                               | 7.51                                | 2.62                          | 0.94                          | 0.84          | ...        | ...        | ...        | ...                           |                                 |
| WARPJ0111.0-3814 | rp700794n00           | 01 11 05.4                 | -38 14 04                  | 5.30                               | 6.79                                | 1.78                          | 0.83                          | 1.18          | BR         | Y          | ...        | ...                           |                                 |
| WARPJ0111.6-3811 | rp700794n00           | 01 11 36.0                 | -38 11 08                  | 4.25                               | 7.40                                | 1.78                          | 0.91                          | 1.63          | BR         | Y          | CLG        | 0.121                         | VMF 009                         |
| WARPJ0124.4+0921 | rp700976n00           | 01 24 25.2                 | +09 21 40                  | 5.36                               | 6.17                                | 4.7                           | 0.82                          | 1.05          | ...        | ...        | star       | ...                           | GS 00614-00801                  |
| WARPJ0124.7+0929 | rp700976n00           | 01 24 46.6                 | +09 29 35                  | 3.12                               | 6.74                                | 4.79                          | 0.9                           | 1.92          | R          | ...        | ...        | ...                           | poss. blend outskirts of NGC524 |
| WARPJ0124.8+0932 | rp700976n00           | 01 24 48.6                 | +09 32 22                  | 20.06                              | 29.60                               | 4.79                          | 3.94                          | 1.39          | ...        | ...        | gal        | 0.0081                        | NGC 524, SHARC                  |
| WARPJ0139.7-6749 | rp300043n00           | 01 39 43.8                 | -67 49 12                  | 18.35                              | 20.04                               | 2.35                          | 2.5                           | 0.33          | ...        | ...        | ...        | ...                           |                                 |
| WARPJ0140.5-6805 | rp300043n00           | 01 40 31.3                 | -68 05 09                  | 12.99                              | 15.57                               | 2.7                           | 1.96                          | 0.26          | ...        | ...        | ...        | ...                           |                                 |
| WARPJ0141.1-6756 | rp300043n00           | 01 41 10.2                 | -67 56 38                  | 4.63                               | 5.43                                | 2.35                          | 0.68                          | 1.06          | ...        | ...        | ...        | ...                           |                                 |
| WARPJ0141.8-6759 | rp300043n00           | 01 41 51.0                 | -67 59 08                  | 7.18                               | 8.54                                | 2.61                          | 1.07                          | 0.81          | ...        | ...        | ...        | ...                           |                                 |
| WARPJ0143.8+0224 | rp700108n00           | 01 43 48.7                 | +02 24 55                  | 4.84                               | 5.72                                | 2.91                          | 0.72                          | 1.08          | R          | ...        | ...        | ...                           |                                 |
| WARPJ0144.5+0212 | rp700108n00           | 01 44 30.3                 | +02 12 24                  | 7.67                               | 14.19                               | 2.91                          | 1.79                          | 1.75          | R          | Y          | CLG        | 0.165                         | VMF 019                         |
| WARPJ0144.5+0222 | rp700108n00           | 01 44 31.9                 | +02 22 17                  | 4.68                               | 5.80                                | 2.91                          | 0.73                          | 1.12          | ...        | Y          | AGN        | 1.024                         |                                 |
| WARPJ0206.1+1512 | rp300003n00           | 02 06 08.6                 | +15 12 32                  | 7.10                               | 7.89                                | 6.18                          | 1.09                          | 1.02          | R          | Y          | gal        | 0.043                         | IC 1777, RIXOS                  |
| WARPJ0206.3+1511 | rp300003n00           | 02 06 23.7                 | +15 11 03                  | 4.26                               | 6.26                                | 6.18                          | 0.86                          | 1.39          | R          | Y          | CLG        | 0.251                         | VMF 022, RIXOS                  |
| WARPJ0206.4+1529 | rp300003n00           | 02 06 24.6                 | +15 29 04                  | 3.75                               | 4.96                                | 6.18                          | 0.69                          | 0.74          | ...        | Y          | NELG       | 0.301                         | RIXOS                           |
| WARPJ0207.3+0231 | rp700432n00           | 02 07 22.5                 | +02 31 31                  | 13.61                              | 15.19                               | 3.11                          | 1.93                          | 0.83          | ...        | ...        | agn        | 0.673                         | MS 0204.8+0217                  |
| WARPJ0207.3+1509 | rp300003n00           | 02 07 21.9                 | +15 09 38                  | 4.06                               | 4.75                                | 6.18                          | 0.66                          | 0.55          | R          | Y          | AGN        | 0.149                         | RIXOS F246 040                  |
| WARPJ0207.9+3518 | rp700977n00           | 02 07 57.9                 | +35 18 34                  | 5.46                               | 6.06                                | 6.26                          | 0.84                          | 1.37          | ...        | Y          | AGN        | 0.188                         |                                 |
| WARPJ0210.4-3929 | rp700027a01           | 02 10 26.7                 | -39 29 27                  | 4.00                               | 7.43                                | 1.43                          | 0.9                           | 1.76          | R          | Y          | CLG        | 0.273:                        | VMF 025                         |
| WARPJ0216.5-1747 | rp900352n00           | 02 16 32.8                 | -17 47 11                  | 7.96                               | 13.42                               | 2.98                          | 1.7                           | 1.6           | R          | Y          | CLG        | 0.578                         |                                 |
| WARPJ0217.4-1800 | rp900352n00           | 02 17 26.5                 | -18 00 10                  | 13.01                              | 14.97                               | 2.98                          | 1.9                           | 1.09          | R          | ...        | blend      | ...                           | SHARC agn+?                     |
| WARPJ0217.7-1750 | rp900352n00           | 02 17 46.5                 | -17 50 25                  | 10.57                              | 11.34                               | 2.56                          | 1.42                          | 1.03          | ...        | ...        | ...        | ...                           |                                 |
| WARPJ0227.7-1014 | rp700114n00           | 02 27 42.8                 | -10 14 17                  | 4.89                               | 7.79                                | 2.51                          | 0.97                          | 1.49          | R          | ...        | ...        | ...                           |                                 |
| WARPJ0228.1-1005 | rp700114n00           | 02 28 11.7                 | -10 05 30                  | 14.11                              | 25.96                               | 2.51                          | 3.25                          | 1.75          | R          | Y          | CLG        | 0.149                         | VMF 026                         |
| WARPJ0229.2-1009 | rp700114n00           | 02 29 13.7                 | -10 09 37                  | 18.27                              | 19.69                               | 2.69                          | 2.48                          | 0.45          | ...        | ...        | ...        | ...                           |                                 |
| WARPJ0229.5-1005 | rp700114n00           | 02 29 35.4                 | -10 05 55                  | 11.01                              | 12.62                               | 2.69                          | 1.59                          | 1.06          | ...        | Y          | ...        | ...                           |                                 |
| WARPJ0235.3-0347 | rp700350n00           | 02 35 19.4                 | -03 47 11                  | 27.03                              | 29.00                               | 2.7                           | 3.65                          | 0.67          | ...        | ...        | agn        | 0.376                         | MS 0232.8-0400                  |
| WARPJ0235.5-0351 | rp700350n00           | 02 35 34.9                 | -03 51 48                  | 6.58                               | 7.24                                | 2.7                           | 0.91                          | 1.04          | ...        | ...        | ...        | ...                           |                                 |
| WARPJ0236.1-5219 | rp701356n00           | 02 36 11.8                 | -52 19 13                  | 5.78                               | 6.38                                | 3.08                          | 0.81                          | 1.09          | R          | ...        | ...        | ...                           |                                 |

Table 2—Continued

| Name<br>(1)      | ROSAT<br>Field<br>(2) | $\alpha$<br>(J2000)<br>(3) | $\delta$<br>(J2000)<br>(4) | $cr_{raw}$<br>[ $10^{-3}$ ]<br>(5) | $cr_{corr}$<br>[ $10^{-3}$ ]<br>(6) | $n_H$<br>[ $10^{20}$ ]<br>(7) | Flux<br>[ $10^{-13}$ ]<br>(8) | Extent<br>(9) | Im<br>(10) | Sp<br>(11) | Id<br>(12) | Redshift/<br>Sp. Type<br>(13) | Other Name/<br>Notes<br>(14) |
|------------------|-----------------------|----------------------------|----------------------------|------------------------------------|-------------------------------------|-------------------------------|-------------------------------|---------------|------------|------------|------------|-------------------------------|------------------------------|
| WARPJ0236.5-5227 | rp701356n00           | 02 36 30.1                 | -52 27 01                  | 5.37                               | 6.48                                | 3.08                          | 0.82                          | 0.64          | ...        | ...        | ...        | ...                           | ...                          |
| WARPJ0236.8-5203 | rp701356n00           | 02 36 51.6                 | -52 03 00                  | 137.13                             | 145.21                              | 3.07                          | 18.44                         | 1.06          | ...        | ...        | star       | M2                            | EXO 0235.2-5216              |
| WARPJ0237.0-5223 | rp701356n00           | 02 37 01.9                 | -52 23 47                  | 56.27                              | 59.69                               | 3.07                          | 7.58                          | 0.12          | ...        | ...        | agn        | 0.113                         | EXO 0235.3-5236              |
| WARPJ0237.2-5227 | rp701356n00           | 02 37 13.6                 | -52 27 32                  | 16.11                              | 17.39                               | 3.07                          | 2.21                          | 0.51          | ...        | ...        | ...        | ...                           | ...                          |
| WARPJ0238.0-5224 | rp701356n00           | 02 38 01.2                 | -52 24 41                  | 30.40                              | 40.67                               | 3.07                          | 5.17                          | 1.28          | R          | Y          | CLG        | 0.135                         | A3038, VMF 028, SHARC        |
| WARPJ0250.0+1908 | rp700920n00           | 02 50 03.5                 | +19 08 00                  | 6.85                               | 11.55                               | 9.87                          | 1.75                          | 1.56          | BR         | Y          | CLG        | 0.122                         | SHARC                        |
| WARPJ0255.0+0017 | rp701403n00           | 02 55 01.3                 | +00 17 49                  | 21.07                              | 22.68                               | 6.48                          | 3.16                          | 1.04          | R          | ...        | ...        | ...                           | ...                          |
| WARPJ0255.0+0025 | rp701403n00           | 02 55 05.7                 | +00 25 26                  | 33.47                              | 35.76                               | 6.64                          | 5                             | 0.99          | ...        | Y          | qso        | 0.354                         | US 3333                      |
| WARPJ0256.0+0015 | rp701403n00           | 02 56 04.0                 | +00 15 55                  | 5.43                               | 7.82                                | 6.64                          | 1.09                          | 1.35          | R          | Y          | BLEND      | ...                           | NELG (z=0.14) + ?            |
| WARPJ0337.4-2518 | rp300079n00           | 03 37 28.6                 | -25 18 48                  | 4.80                               | 6.05                                | 1.55                          | 0.73                          | 1.16          | R          | ...        | ...        | ...                           | ...                          |
| WARPJ0337.5-2518 | rp300079n00           | 03 37 35.2                 | -25 18 10                  | 12.11                              | 14.02                               | 1.55                          | 1.71                          | 1.08          | R          | ...        | ...        | ...                           | SHARC                        |
| WARPJ0337.6-2523 | rp300079n00           | 03 37 37.9                 | -25 23 23                  | 5.76                               | 6.55                                | 1.55                          | 0.8                           | 1.05          | R          | ...        | ...        | ...                           | ...                          |
| WARPJ0338.4-2524 | rp300079n00           | 03 38 27.6                 | -25 23 59                  | 5.15                               | 5.75                                | 1.55                          | 0.7                           | 0.86          | ...        | ...        | ...        | ...                           | ...                          |
| WARPJ0338.6-2529 | rp300079n00           | 03 38 36.0                 | -25 29 10                  | 8.17                               | 9.55                                | 1.55                          | 1.16                          | 0.87          | ...        | ...        | ...        | ...                           | ...                          |
| WARPJ0347.6-1217 | rp900492n00           | 03 47 40.7                 | -12 16 59                  | 3.65                               | 5.04                                | 3.84                          | 0.65                          | 1.22          | R          | ...        | ...        | ...                           | ...                          |
| WARPJ0347.8-1217 | rp900492n00           | 03 47 50.4                 | -12 17 01                  | 3.95                               | 5.06                                | 3.84                          | 0.66                          | 1.08          | R          | Y          | ...        | ...                           | ...                          |
| WARPJ0348.1-1201 | rp900492n00           | 03 48 08.7                 | -12 01 34                  | 5.05                               | 7.40                                | 3.8                           | 0.96                          | 1.38          | R          | Y          | CLG        | 0.488                         | ...                          |
| WARPJ0349.3-1205 | rp900492n00           | 03 49 18.7                 | -12 05 43                  | 6.41                               | 7.85                                | 3.8                           | 1.02                          | 0.94          | ...        | ...        | ...        | ...                           | ...                          |
| WARPJ0411.5-1717 | rp900246n00           | 04 11 34.7                 | -17 17 25                  | 5.91                               | 6.88                                | 2.52                          | 0.86                          | 1.05          | ...        | Y          | AGN        | ...                           | ...                          |
| WARPJ0411.9-1728 | rp900246n00           | 04 11 58.4                 | -17 28 04                  | 8.35                               | 9.80                                | 2.49                          | 1.22                          | 1.1           | ...        | ...        | ...        | ...                           | ...                          |
| WARPJ0421.7-3847 | rp700026n00           | 04 21 47.1                 | -38 47 47                  | 4.41                               | 6.04                                | 1.9                           | 0.74                          | 1.26          | R          | ...        | ...        | ...                           | ...                          |
| WARPJ0421.8-3833 | rp700026n00           | 04 21 52.5                 | -38 33 00                  | 3.78                               | 5.59                                | 1.9                           | 0.69                          | 0.53          | ...        | ...        | ...        | ...                           | ...                          |
| WARPJ0422.3-3832 | rp700026n00           | 04 22 20.8                 | -38 32 20                  | 4.84                               | 6.72                                | 1.9                           | 0.83                          | 6.79          | ...        | ...        | qso        | 0.482                         | MS 0420.6-3839               |
| WARPJ0440.8-1635 | rp900017n00           | 04 40 53.2                 | -16 35 22                  | 9.93                               | 10.75                               | 4.69                          | 1.43                          | 0.15          | R          | ...        | star       | G0                            | 1E 0438.6-1641               |
| WARPJ0441.0-1616 | rp900017n00           | 04 41 05.2                 | -16 16 08                  | 9.43                               | 10.92                               | 4.69                          | 1.45                          | 1.03          | R          | ...        | ...        | ...                           | ...                          |
| WARPJ0951.7-0128 | rp700908n00           | 09 51 47.0                 | -01 28 30                  | 3.00                               | 5.54                                | 3.84                          | 0.72                          | 1.73          | R          | Y          | CLG        | 0.568                         | VMF 076                      |
| WARPJ0952.1-0148 | rp700908n00           | 09 52 08.5                 | -01 48 20                  | 3.78                               | 6.23                                | 3.84                          | 0.81                          | 1.56          | R          | ...        | ...        | ...                           | VMF 077                      |
| WARPJ0952.5-0137 | rp700908n00           | 09 52 34.8                 | -01 37 53                  | 4.05                               | 5.31                                | 3.84                          | 0.69                          | 1.22          | ...        | ...        | ...        | ...                           | ...                          |
| WARPJ0952.7-0130 | rp700908n00           | 09 52 43.3                 | -01 30 47                  | 9.76                               | 11.50                               | 3.84                          | 1.49                          | 1.1           | ...        | Y          | BLEND      | ...                           | QSO (z=1.26)+K star          |
| WARPJ1112.8-2619 | rp201019n00           | 11 12 50.5                 | -26 19 07                  | 8.63                               | 10.46                               | 5.47                          | 1.42                          | 1.12          | IR         | ...        | ...        | ...                           | ...                          |
| WARPJ1113.0-2615 | rp201019n00           | 11 13 05.7                 | -26 15 36                  | 4.10                               | 5.42                                | 5.47                          | 0.74                          | 1.21          | IR         | Y          | CLG        | 0.725                         | ...                          |
| WARPJ1259.1+3501 | rp600164n00           | 12 59 09.2                 | +35 01 15                  | 5.42                               | 6.29                                | 1.22                          | 0.76                          | 0.83          | ...        | ...        | ...        | ...                           | ...                          |
| WARPJ1259.5+1226 | rp400116n00           | 12 59 33.3                 | +12 26 47                  | 4.05                               | 8.07                                | 2.27                          | 1                             | 1.82          | R          | ...        | ...        | ...                           | ...                          |
| WARPJ1316.4+4454 | rp900325n00           | 13 16 25.7                 | +44 54 18                  | 21.06                              | 23.87                               | 1.45                          | 2.9                           | 0.93          | ...        | ...        | ...        | ...                           | ...                          |
| WARPJ1317.4+4456 | rp900325n00           | 13 17 28.3                 | +44 56 40                  | 5.41                               | 6.97                                | 1.54                          | 0.85                          | 1.19          | ...        | ...        | ...        | ...                           | ...                          |

Table 2—Continued

| Name<br>(1)      | ROSAT<br>Field<br>(2) | $\alpha$<br>(J2000)<br>(3) | $\delta$<br>(J2000)<br>(4) | $cr_{raw}$<br>[ $10^{-3}$ ]<br>(5) | $cr_{corr}$<br>[ $10^{-3}$ ]<br>(6) | $n_H$<br>[ $10^{20}$ ]<br>(7) | Flux<br>[ $10^{-13}$ ]<br>(8) | Extent<br>(9) | Im<br>(10) | Sp<br>(11) | Id<br>(12) | Redshift/<br>Sp. Type<br>(13) | Other Name/<br>Notes<br>(14) |
|------------------|-----------------------|----------------------------|----------------------------|------------------------------------|-------------------------------------|-------------------------------|-------------------------------|---------------|------------|------------|------------|-------------------------------|------------------------------|
| WARPJ1318.6+4500 | rp900325n00           | 13 18 39.9                 | +45 00 48                  | 4.71                               | 6.04                                | 1.78                          | 0.74                          | 1.19          | R          | Y          | BLEND      | 0.173                         | AGN (z=0.173:) + ?           |
| WARPJ1328.9+0112 | rp201070n00           | 13 28 56.1                 | +01 12 15                  | 4.36                               | 6.76                                | 1.85                          | 0.83                          | 3.15          | R          | ...        | ...        | ...                           |                              |
| WARPJ1343.0-0013 | rp701000a01           | 13 43 02.6                 | -00 13 01                  | 7.14                               | 8.63                                | 1.91                          | 1.06                          | 3             | ...        | ...        | ...        | ...                           |                              |
| WARPJ1348.5+0757 | rp300028n00           | 13 48 34.9                 | +07 57 37                  | 7.31                               | 8.09                                | 2                             | 1                             | 0.08          | ...        | ...        | star       | F5                            | HD 120317                    |
| WARPJ1356.1+2606 | rp201037n00           | 13 56 09.6                 | +26 06 41                  | 4.79                               | 6.23                                | 1.3                           | 0.75                          | 1.2           | R          | Y          | BLEND      | 1.32                          | QSO (z=1.32) + ?             |
| WARPJ1356.3+2552 | rp201037n00           | 13 56 22.0                 | +25 52 49                  | 4.67                               | 5.44                                | 1.34                          | 0.66                          | 1.06          | R          | ...        | ...        | ...                           |                              |
| WARPJ1406.2+2830 | rp700061n00           | 14 06 16.1                 | +28 30 55                  | 4.74                               | 7.07                                | 1.46                          | 0.86                          | 1.39          | R          | Y          | CLG        | 0.546                         | VMF 153                      |
| WARPJ1406.9+2834 | rp700061n00           | 14 06 55.4                 | +28 34 25                  | 11.32                              | 19.06                               | 1.46                          | 2.31                          | 1.58          | BR         | Y          | CLG        | 0.117                         | VMF 154, SHARC               |
| WARPJ1407.3+2818 | rp700061n00           | 14 07 19.5                 | +28 18 19                  | 14.81                              | 16.50                               | 1.46                          | 2                             | 0.48          | ...        | ...        | qso        | 1.121                         | CRSS J1407.3+2818            |
| WARPJ1407.7+2830 | rp700061n00           | 14 07 45.5                 | +28 30 31                  | 26.86                              | 30.94                               | 1.46                          | 3.75                          | 0.81          | R          | ...        | qso        | 0.642                         | CRSS J1407.7+2830, FIRST     |
| WARPJ1415.1+3612 | rp600462n00           | 14 15 11.1                 | +36 12 03                  | 6.30                               | 9.13                                | 1.14                          | 1.1                           | 1.36          | R          | ...        | CLG        | [0.7]                         | FIRST                        |
| WARPJ1415.2+3608 | rp600462n00           | 14 15 12.4                 | +36 08 09                  | 14.25                              | 15.38                               | 1.14                          | 1.85                          | 0.99          | ...        | ...        | ...        | ...                           |                              |
| WARPJ1415.5+1131 | rp700122n00           | 14 15 31.8                 | +11 31 57                  | 10.34                              | 11.81                               | 1.8                           | 1.45                          | 1.06          | ...        | ...        | qso        | 0.256                         | CRSS J1415.5+1131            |
| WARPJ1417.3+2505 | rp150071n00           | 14 17 22.1                 | +25 05 22                  | 13.48                              | 14.80                               | 1.58                          | 1.8                           | 0.44          | ...        | ...        | ...        | ...                           |                              |
| WARPJ1417.3+2513 | rp150071n00           | 14 17 23.2                 | +25 13 41                  | 5.26                               | 6.69                                | 1.58                          | 0.81                          | 0.21          | ...        | ...        | qso        | 0.56                          | 2E 1416.6+2523               |
| WARPJ1418.5+2511 | rp150071n00           | 14 18 31.8                 | +25 10 59                  | 39.21                              | 48.92                               | 1.93                          | 6.02                          | 1.18          | R          | Y          | CLG        | 0.296                         | VMF 159, SHARC               |
| WARPJ1418.6-1306 | rp700527n00           | 14 18 38.1                 | -13 06 36                  | 5.47                               | 6.23                                | 6.29                          | 0.86                          | 1.02          | ...        | ...        | ...        | ...                           |                              |
| WARPJ1418.9+2509 | rp150071n00           | 14 18 58.2                 | +25 09 49                  | 7.58                               | 8.54                                | 1.93                          | 1.05                          | 0.73          | ...        | ...        | qso        | 0.674                         | [HB89] 1416+254              |
| WARPJ1419.5-1321 | rp700527n00           | 14 19 33.2                 | -13 21 13                  | 4.54                               | 6.82                                | 7.11                          | 0.97                          | 1.38          | R          | ...        | ...        | ...                           |                              |
| WARPJ1419.6-1316 | rp700527n00           | 14 19 39.3                 | -13 16 35                  | 6.11                               | 7.01                                | 7.11                          | 0.99                          | 1.05          | R          | ...        | ...        | ...                           |                              |
| WARPJ1435.4+4845 | rp600448n00           | 14 35 29.0                 | +48 45 17                  | 4.41                               | 6.48                                | 2.05                          | 0.8                           | 1.38          | ...        | ...        | gal        | 0.0072                        | NGC 5689                     |
| WARPJ1505.7+5549 | rp600119n00           | 15 05 43.9                 | +55 49 33                  | 8.57                               | 10.05                               | 1.47                          | 1.22                          | 1.08          | ...        | ...        | ...        | ...                           |                              |
| WARPJ1506.8+5532 | rp600119n00           | 15 06 51.1                 | +55 32 06                  | 5.81                               | 7.47                                | 1.47                          | 0.91                          | 0.84          | ...        | ...        | ...        | ...                           |                              |
| WARPJ1513.5+3846 | rp200905n00           | 15 13 32.3                 | +38 46 00                  | 6.31                               | 7.33                                | 1.39                          | 0.89                          | 0.41          | R          | ...        | ...        | ...                           |                              |
| WARPJ1513.8+4400 | rp200965n00           | 15 13 48.9                 | +44 00 06                  | 5.33                               | 6.60                                | 1.95                          | 0.81                          | 1.16          | R          | ...        | ...        | ...                           |                              |
| WARPJ1515.6+4411 | rp200965n00           | 15 15 39.1                 | +44 11 29                  | 9.07                               | 10.28                               | 2.04                          | 1.27                          | 1.04          | R          | ...        | ...        | ...                           |                              |
| WARPJ1517.0+3140 | rp201018n00           | 15 17 03.6                 | +31 40 45                  | 5.33                               | 6.13                                | 1.91                          | 0.75                          | 0.97          | R          | ...        | ...        | ...                           | SHARC                        |
| WARPJ1517.2+3141 | rp201018n00           | 15 17 13.0                 | +31 41 25                  | 5.26                               | 6.16                                | 1.91                          | 0.76                          | 0.67          | R          | ...        | star       | G5                            | PPM 78477, FIRST             |
| WARPJ1519.3+3139 | rp201018n00           | 15 19 19.6                 | +31 39 07                  | 5.40                               | 6.07                                | 1.9                           | 0.75                          | 0.04          | R          | ...        | ...        | ...                           |                              |
| WARPJ1524.9+4143 | rp701405n00           | 15 24 59.9                 | +41 43 37                  | 9.04                               | 10.26                               | 2.08                          | 1.27                          | 1.05          | ...        | ...        | ...        | ...                           | FIRST                        |
| WARPJ1525.8+4139 | rp701405n00           | 15 25 49.1                 | +41 39 28                  | 4.13                               | 5.82                                | 2.08                          | 0.72                          | 1.31          | ...        | ...        | BLEND      | ...                           |                              |
| WARPJ1525.9+4148 | rp701405n00           | 15 25 58.2                 | +41 48 36                  | 8.00                               | 9.17                                | 2.08                          | 1.13                          | 1.07          | ...        | ...        | ...        | ...                           |                              |
| WARPJ1527.1+4133 | rp701405n00           | 15 27 08.8                 | +41 33 12                  | 5.72                               | 7.75                                | 2.08                          | 0.96                          | 0.31          | ...        | ...        | star       | G5                            | HD 137896, FIRST             |
| WARPJ1548.8+2120 | rp701373n00           | 15 48 51.9                 | +21 20 27                  | 7.42                               | 8.67                                | 4.3                           | 1.14                          | 1.05          | ...        | ...        | ...        | ...                           |                              |
| WARPJ1549.7+2114 | rp701373n00           | 15 49 43.2                 | +21 14 02                  | 16.45                              | 18.61                               | 4.3                           | 2.45                          | 1.12          | ...        | ...        | ...        | ...                           |                              |

Table 2—Continued

| Name<br>(1)      | ROSAT<br>Field<br>(2) | $\alpha$<br>(J2000)<br>(3) | $\delta$<br>(J2000)<br>(4) | $cr_{raw}$<br>[ $10^{-3}$ ]<br>(5) | $cr_{corr}$<br>[ $10^{-3}$ ]<br>(6) | $n_H$<br>[ $10^{20}$ ]<br>(7) | Flux<br>[ $10^{-13}$ ]<br>(8) | Extent<br>(9) | Im<br>(10) | Sp<br>(11) | Id<br>(12) | Redshift/<br>Sp. Type<br>(13) | Other Name/<br>Notes<br>(14) |
|------------------|-----------------------|----------------------------|----------------------------|------------------------------------|-------------------------------------|-------------------------------|-------------------------------|---------------|------------|------------|------------|-------------------------------|------------------------------|
| WARPJ1550.2+2124 | rp701373n00           | 15 50 15.1                 | +21 24 30                  | 4.66                               | 5.05                                | 4.3                           | 0.66                          | 1.03          | ...        | ...        | ...        | ...                           | ...                          |
| WARPJ1552.0+2013 | rp701213n00           | 15 52 02.5                 | +20 13 58                  | 70.44                              | 80.42                               | 3.7                           | 10.4                          | 1.07          | R          | ...        | qso        | 0.25                          | [HB89] 1549+203              |
| WARPJ1552.2+2013 | rp701213n00           | 15 52 12.5                 | +20 13 32                  | 11.88                              | 25.70                               | 3.7                           | 3.32                          | 2.04          | BR         | Y          | CLG        | 0.135                         | VMF 175, SHARC               |
| WARPJ1552.4+2007 | rp701213n00           | 15 52 29.8                 | +20 07 18                  | 24.63                              | 28.09                               | 3.7                           | 3.63                          | 1.06          | R          | ...        | ...        | ...                           | RadioS                       |
| WARPJ1558.1+3500 | rp700096n00           | 15 58 09.7                 | +35 00 52                  | 5.43                               | 6.99                                | 2.03                          | 0.86                          | 1.94          | R          | ...        | ...        | ...                           | ...                          |
| WARPJ1558.7+3511 | rp700096n00           | 15 58 43.6                 | +35 11 19                  | 4.13                               | 6.58                                | 1.86                          | 0.81                          | 1.45          | R          | ...        | ...        | ...                           | ...                          |
| WARPJ1655.4-0820 | rp200125n00           | 16 55 29.3                 | -08 20 00                  | 1268.80                            | 1344.76                             | 13.38                         | 222.46                        | 1.28          | ...        | ...        | star       | M3Ve                          | V1054 Oph                    |
| WARPJ1656.1-0819 | rp200125n00           | 16 56 11.7                 | -08 19 10                  | 5.00                               | 5.98                                | 13.38                         | 0.99                          | 0.01          | ...        | ...        | ...        | ...                           | ...                          |
| WARPJ1716.5+4302 | rp300180n00           | 17 16 32.6                 | +43 02 27                  | 53.61                              | 57.08                               | 2.19                          | 7.08                          | 0.67          | ...        | Y          | STAR       | G/K                           | in NGC 6341                  |
| WARPJ1841.5+5531 | rp201505n00           | 18 41 31.1                 | +55 31 17                  | 4.60                               | 5.27                                | 4.95                          | 0.7                           | 1.68          | ...        | Y          | AGN        | ...                           | ...                          |
| WARPJ1841.8+5540 | rp201505n00           | 18 41 50.9                 | +55 40 48                  | 6.51                               | 7.78                                | 4.95                          | 1.04                          | 1.08          | ...        | Y          | ...        | ...                           | RadioS                       |
| WARPJ1842.7+5529 | rp201505n00           | 18 42 43.9                 | +55 29 22                  | 31.19                              | 33.25                               | 4.95                          | 4.45                          | 1.09          | ...        | Y          | ...        | ...                           | RadioS                       |
| WARPJ1843.4+5527 | rp201505n00           | 18 43 26.7                 | +55 27 44                  | 4.36                               | 5.71                                | 4.95                          | 0.76                          | 1.23          | ...        | Y          | BLEND      | ...                           | ...                          |
| WARPJ2037.6-0125 | rp300218n00           | 20 37 36.7                 | -01 25 28                  | 17.70                              | 19.07                               | 7.02                          | 2.69                          | 1.02          | ...        | Y          | AGN        | 0.132                         | ...                          |
| WARPJ2038.3-0106 | rp300218n00           | 20 38 20.2                 | -01 06 19                  | 9.96                               | 11.40                               | 7.02                          | 1.61                          | 4.85          | ...        | ...        | star       | G8/K0                         | HD 196574                    |
| WARPJ2038.4-0125 | rp300218n00           | 20 38 29.6                 | -01 25 11                  | 2.65                               | 4.84                                | 7.02                          | 0.68                          | 1.71          | BR         | Y          | CLG        | 0.679                         | ...                          |
| WARPJ2038.7-0114 | rp300218n00           | 20 38 47.9                 | -01 14 24                  | 15.85                              | 17.46                               | 7.02                          | 2.47                          | 1.06          | ...        | ...        | ...        | ...                           | ...                          |
| WARPJ2107.6-0512 | rp300389n00           | 21 07 36.6                 | -05 12 11                  | 11.02                              | 12.46                               | 5.57                          | 1.7                           | 1.05          | ...        | ...        | ...        | ...                           | ...                          |
| WARPJ2108.6-1316 | rp201007n00           | 21 08 40.7                 | -13 16 46                  | 7.55                               | 8.60                                | 4.09                          | 1.12                          | 1.03          | ...        | ...        | ...        | ...                           | ...                          |
| WARPJ2108.8-0516 | rp300389n00           | 21 08 51.0                 | -05 16 32                  | 9.33                               | 13.71                               | 5.57                          | 1.86                          | 1.4           | R          | Y          | CLG        | 0.317                         | VMF 200                      |
| WARPJ2115.2+0608 | rp700006n00           | 21 15 16.4                 | +06 08 43                  | 10.95                              | 12.83                               | 6.62                          | 1.79                          | 1.09          | ...        | Y          | qso        | 0.398                         | [HB89] 2112+059              |
| WARPJ2126.9+1257 | rp900345n00           | 21 26 54.5                 | +12 57 39                  | 8.18                               | 10.03                               | 6.38                          | 1.39                          | 1.1           | ...        | Y          | AGN        | 0.82                          | ...                          |
| WARPJ2127.0+1251 | rp900345n00           | 21 27 02.4                 | +12 51 10                  | 5.20                               | 6.74                                | 6.38                          | 0.94                          | 0.61          | ...        | Y          | AGN        | 0.22                          | ...                          |
| WARPJ2158.4-1450 | rp701420n00           | 21 58 28.7                 | -14 50 34                  | 4.14                               | 7.24                                | 3.75                          | 0.94                          | 1.63          | R          | Y          | BLEND      | 1.075                         | QSO (z=1.08) + ?             |
| WARPJ2158.9-1452 | rp701420n00           | 21 58 55.2                 | -14 52 53                  | 3.95                               | 5.13                                | 3.75                          | 0.66                          | 1.11          | R          | ...        | ...        | ...                           | ...                          |
| WARPJ2223.5-0218 | rp701018n00           | 22 23 32.8                 | -02 18 04                  | 9.68                               | 11.11                               | 4.95                          | 1.49                          | 1.07          | ...        | ...        | star       | F8                            | HD 212337                    |
| WARPJ2223.8-0206 | rp701018n00           | 22 23 48.6                 | -02 06 19                  | 19.83                              | 26.06                               | 4.95                          | 3.49                          | 1.24          | R          | ...        | agn        | 0.056                         | 3C 445, SHARC, FIRST         |
| WARPJ2224.3-0218 | rp701018n00           | 22 24 22.7                 | -02 18 33                  | 5.92                               | 7.77                                | 4.95                          | 1.04                          | 1.23          | R          | ...        | ...        | ...                           | ...                          |
| WARPJ2225.0-0457 | rp900337n00           | 22 25 00.5                 | -04 57 51                  | 5.67                               | 6.55                                | 5.07                          | 0.88                          | 0.77          | R          | ...        | ...        | ...                           | ...                          |
| WARPJ2239.4-0547 | rp701206n00           | 22 39 24.8                 | -05 47 10                  | 15.81                              | 21.80                               | 4.01                          | 2.84                          | 1.3           | BR         | Y          | CLG        | 0.242                         | A2465S, VMF 208              |
| WARPJ2239.5-0600 | rp701206n00           | 22 39 35.4                 | -06 00 17                  | 3.33                               | 5.16                                | 3.96                          | 0.67                          | 1.46          | BR         | Y          | CLG        | 0.174                         | VMF 209                      |
| WARPJ2239.6-0543 | rp701206n00           | 22 39 39.6                 | -05 43 15                  | 17.60                              | 30.48                               | 4.01                          | 3.97                          | 1.65          | BR         | Y          | CLG        | 0.243                         | A2465N, VMF 210              |
| WARPJ2253.5+2852 | rp400293n00           | 22 53 35.2                 | +28 52 11                  | 5.34                               | 6.19                                | 5.6                           | 0.84                          | 0.77          | R          | ...        | ...        | ...                           | ...                          |
| WARPJ2253.6+2913 | rp400293n00           | 22 53 37.6                 | +29 13 13                  | 21.09                              | 23.00                               | 5.68                          | 3.14                          | 0.74          | ...        | ...        | ...        | ...                           | ...                          |
| WARPJ2254.1+1606 | rp900339n00           | 22 54 10.9                 | +16 06 56                  | 9.19                               | 9.92                                | 6.54                          | 1.38                          | 1.04          | ...        | ...        | ...        | ...                           | ...                          |

Table 2—Continued

| Name<br>(1)      | ROSAT<br>Field<br>(2) | $\alpha$<br>(J2000)<br>(3) | $\delta$<br>(J2000)<br>(4) | $cr_{raw}$<br>[ $10^{-3}$ ]<br>(5) | $cr_{corr}$<br>[ $10^{-3}$ ]<br>(6) | $n_H$<br>[ $10^{20}$ ]<br>(7) | Flux<br>[ $10^{-13}$ ]<br>(8) | Extent<br>(9) | Im<br>(10) | Sp<br>(11) | Id<br>(12) | Redshift/<br>Sp. Type<br>(13) | Other Name/<br>Notes<br>(14) |
|------------------|-----------------------|----------------------------|----------------------------|------------------------------------|-------------------------------------|-------------------------------|-------------------------------|---------------|------------|------------|------------|-------------------------------|------------------------------|
| WARPJ2254.8+1604 | rp900339n00           | 22 54 49.8                 | +16 04 21                  | 10.28                              | 11.28                               | 6.54                          | 1.57                          | 0.99          | ...        | Y          | ...        | ...                           |                              |
| WARPJ2255.4+2905 | rp400293n00           | 22 55 26.1                 | +29 05 28                  | 4.26                               | 5.42                                | 5.68                          | 0.74                          | 1.12          | R          | ...        | ...        | ...                           |                              |
| WARPJ2302.7+0845 | rp700423n00           | 23 02 46.4                 | +08 45 20                  | 3.80                               | 5.23                                | 5.28                          | 0.7                           | 0.19          | R          | ...        | ...        | ...                           |                              |
| WARPJ2302.8+0843 | rp700423n00           | 23 02 48.1                 | +08 43 50                  | 4.63                               | 5.24                                | 4.86                          | 0.7                           | 0.92          | R          | Y          | CLG        | 0.722                         |                              |
| WARPJ2302.9+0839 | rp700423n00           | 23 02 54.7                 | +08 39 04                  | 4.47                               | 5.57                                | 4.86                          | 0.74                          | 0.22          | R          | ...        | ...        | ...                           |                              |
| WARPJ2303.0+0846 | rp700423n00           | 23 03 01.0                 | +08 46 55                  | 5.45                               | 6.04                                | 4.86                          | 0.81                          | 0.71          | ...        | ...        | ...        | ...                           |                              |
| WARPJ2304.0-0837 | rp701250n00           | 23 04 00.5                 | -08 37 52                  | 5.35                               | 6.55                                | 3.51                          | 0.84                          | 0.01          | ...        | ...        | ...        | ...                           |                              |
| WARPJ2319.5+1226 | rp200474n00           | 23 19 34.6                 | +12 26 21                  | 21.23                              | 31.72                               | 4.42                          | 4.18                          | 1.42          | R          | Y          | CLG        | 0.124                         | VMF 217, RIXOS               |
| WARPJ2320.7+1659 | rp600439n00           | 23 20 46.1                 | +16 59 45                  | 3.43                               | 5.28                                | 4.38                          | 0.7                           | 1.44          | R          | Y          | BLEND      | 0.499                         | AGN (z=1.8) + CLG (z=0.50)   |
| WARPJ2320.9+1715 | rp600439n00           | 23 20 57.8                 | +17 15 10                  | 14.33                              | 15.56                               | 4.68                          | 2.07                          | 0.79          | ...        | ...        | star       | A9/F0                         | HD 220091                    |

Table 3. Other Sources

| Name<br>(1)      | ROSAT<br>Field<br>(2) | $\alpha$<br>(J2000)<br>(3) | $\delta$<br>(J2000)<br>(4) | $cr_{raw}$<br>[ $10^{-3}$ ]<br>(5) | $cr_{corr}$<br>[ $10^{-3}$ ]<br>(6) | $n_H$<br>[ $10^{20}$ ]<br>(7) | Flux<br>[ $10^{-13}$ ]<br>(8) | Extent<br>(9) | Im<br>(10) | Sp<br>(11) | Id<br>(12) | Redshift/<br>Sp. Type<br>(13) | Other Name/<br>Notes<br>(14) |
|------------------|-----------------------|----------------------------|----------------------------|------------------------------------|-------------------------------------|-------------------------------|-------------------------------|---------------|------------|------------|------------|-------------------------------|------------------------------|
| WARPJ0019.5+2156 | rp400322n00           | 00 19 34.7                 | +21 56 24                  | 3.26                               | 4.09                                | 4.28                          | 0.54                          | 1.16          | R          | ...        | ...        | ...                           |                              |
| WARPJ0019.8+2202 | rp400322n00           | 00 19 49.4                 | +22 02 51                  | 4.03                               | 4.89                                | 4.14                          | 0.64                          | 1.13          | R          | Y          | BLEND      | ...                           | M star+galaxy IC 1541        |
| WARPJ0038.5+3058 | rp201045n00           | 00 38 34.2                 | +30 58 22                  | 3.24                               | 3.79                                | 5.6                           | 0.52                          | 0.77          | ...        | Y          | QSO        | 1.326                         |                              |
| WARPJ0045.8+0107 | rp700377n00           | 00 45 50.3                 | +01 07 24                  | 3.45                               | 4.35                                | 2.62                          | 0.55                          | 0.94          | R          | ...        | ...        | ...                           |                              |
| WARPJ0110.7-3813 | rp700794n00           | 01 10 44.9                 | -38 13 28                  | 3.54                               | 4.48                                | 1.78                          | 0.55                          | 1.16          | R          | ...        | ...        | ...                           |                              |
| WARPJ0207.1+1504 | rp300003n00           | 02 07 06.8                 | +15 04 54                  | 3.23                               | 4.30                                | 6.18                          | 0.59                          | 0.72          | R          | ...        | ...        | ...                           | RIXOS                        |
| WARPJ0216.9-1753 | rp900352n00           | 02 16 57.9                 | -17 53 58                  | 3.17                               | 3.84                                | 2.98                          | 0.49                          | 1.12          | R          | ...        | ...        | ...                           |                              |
| WARPJ0234.2-0356 | rp700350n00           | 02 34 13.3                 | -03 56 51                  | 3.62                               | 5.11                                | 2.59                          | 0.64                          | 1.31          | R          | Y          | CLG        | 0.447                         |                              |
| WARPJ0236.0-5224 | rp701356n00           | 02 36 04.2                 | -52 24 50                  | 3.47                               | 4.06                                | 3.08                          | 0.52                          | 1.09          | R          | ...        | ...        | ...                           | VMF 027                      |
| WARPJ0236.7-5209 | rp701356n00           | 02 36 47.9                 | -52 09 22                  | 3.58                               | 4.01                                | 3.07                          | 0.51                          | 0.14          | R          | ...        | ...        | ...                           |                              |
| WARPJ0255.3+0004 | rp701403n00           | 02 55 23.1                 | +00 04 38                  | 3.63                               | 4.58                                | 6.48                          | 0.64                          | 1.18          | R          | ...        | ...        | ...                           |                              |
| WARPJ0255.4-0002 | rp701403n00           | 02 55 27.9                 | -00 02 24                  | 3.19                               | 4.58                                | 6.48                          | 0.64                          | 1.35          | R          | ...        | blend      | ...                           | AGN (Q 0252-0014)+?          |
| WARPJ0347.8-1158 | rp900492n00           | 03 47 50.3                 | -11 58 43                  | 3.00                               | 3.91                                | 3.8                           | 0.51                          | 1.04          | R          | ...        | ...        | ...                           |                              |
| WARPJ0412.4-1724 | rp900246n00           | 04 12 30.0                 | -17 24 38                  | 3.82                               | 4.92                                | 2.52                          | 0.61                          | 1.18          | R          | ...        | ...        | ...                           |                              |
| WARPJ0414.4-1236 | rp900242n00           | 04 14 25.2                 | -12 36 41                  | 3.97                               | 4.61                                | 3.7                           | 0.6                           | 0.03          | R          | ...        | ...        | ...                           |                              |
| WARPJ0414.7-1240 | rp900242n00           | 04 14 43.2                 | -12 40 04                  | 3.01                               | 3.71                                | 3.7                           | 0.48                          | 1.08          | R          | ...        | ...        | ...                           |                              |
| WARPJ0440.6-1636 | rp900017n00           | 04 40 39.1                 | -16 36 05                  | 3.15                               | 4.23                                | 4.69                          | 0.56                          | 1.24          | R          | ...        | ...        | ...                           |                              |
| WARPJ1311.1+3711 | rp700796n00           | 13 11 11.0                 | +37 11 57                  | 3.46                               | 3.99                                | 1.11                          | 0.48                          | 1.16          | R          | ...        | ...        | ...                           |                              |
| WARPJ1318.8+4457 | rp900325n00           | 13 18 52.8                 | +44 57 42                  | 3.73                               | 4.26                                | 1.54                          | 0.52                          | 1.03          | R          | ...        | ...        | ...                           |                              |
| WARPJ1349.0+0750 | rp300028n00           | 13 49 02.3                 | +07 50 44                  | 3.17                               | 3.85                                | 2.05                          | 0.47                          | 1.06          | R          | ...        | ...        | ...                           |                              |
| WARPJ1407.6+3415 | rp700117n00           | 14 07 40.5                 | +34 15 18                  | 3.40                               | 4.73                                | 1.2                           | 0.57                          | 1.3           | R          | Y          | CLG        | 0.577                         |                              |
| WARPJ1407.7+2824 | rp700061n00           | 14 07 45.6                 | +28 24 42                  | 3.06                               | 4.32                                | 1.46                          | 0.52                          | 0.92          | R          | ...        | qso        | 1.127                         | CRSS J1407.7+2824            |
| WARPJ1415.0+1119 | rp700122n00           | 14 15 04.5                 | +11 19 35                  | 2.67                               | 3.65                                | 1.8                           | 0.45                          | 1.02          | R          | ...        | qso        | 0.538                         | CRSS J1415.0+1119            |
| WARPJ1415.2+1119 | rp700122n00           | 14 15 16.8                 | +11 19 30                  | 2.86                               | 4.67                                | 1.8                           | 0.57                          | 1.4           | R          | ...        | star       | G                             | CRSS J1415.2+1119            |
| WARPJ1415.6+3622 | rp600462n00           | 14 15 39.0                 | +36 22 11                  | 4.01                               | 5.10                                | 0.99                          | 0.61                          | 1.19          | R          | ...        | gal        | 0.0159                        | KUG 1413+366                 |
| WARPJ1501.0-0824 | rp200510n00           | 15 01 04.3                 | -08 24 56                  | 3.03                               | 3.42                                | 7.33                          | 0.49                          | 0.69          | R          | N          | CLG?       | 0.51                          | estimated redshift           |
| WARPJ1515.6+4346 | rp200965n00           | 15 15 31.9                 | +43 46 18                  | 15.82                              | 24.48                               | 1.96                          | 2.98                          | 1.48          | R          | Y          | CLG        | 0.135                         | VMF 169                      |
| WARPJ1517.9+3127 | rp201018n00           | 15 17 55.9                 | +31 27 35                  | 3.02                               | 4.57                                | 1.9                           | 0.57                          | 1.43          | R          | Y          | CLG        | 0.744                         | ...                          |
| WARPJ1535.1+2336 | rp701411n00           | 15 35 06.0                 | +23 36 55                  | 4.19                               | 4.59                                | 4.29                          | 0.6                           | 1.19          | ...        | Y          | AGN        | 1.25                          |                              |
| WARPJ1537.7+1201 | rp400117n00           | 15 37 43.0                 | +12 01 14                  | 5.51                               | 10.52                               | 3.44                          | 1.29                          | ...           | R          | Y          | CLG        | 0.136                         | VMF 171                      |
| WARPJ1552.1+2017 | rp701213n00           | 15 52 07.8                 | +20 17 39                  | 3.20                               | 3.72                                | 3.7                           | 0.48                          | 1             | R          | ...        | ...        | ...                           |                              |
| WARPJ1605.2+2541 | rp300021n00           | 16 05 17.2                 | +25 41 23                  | 3.31                               | 4.41                                | 4.62                          | 0.58                          | 0.21          | R          | ...        | qso        | 1.071                         | CRSS J1605.2+2541            |
| WARPJ1605.6+2543 | rp300021n00           | 16 05 39.7                 | +25 43 08                  | 3.38                               | 4.29                                | 4.62                          | 0.57                          | 1.15          | R          | ...        | gal        | 0.278                         | CRSS J1605.6+2543            |
| WARPJ1717.4+4319 | rp300180n00           | 17 17 29.8                 | +43 19 41                  | 3.66                               | 4.45                                | 2.19                          | 0.55                          | 0.4           | ...        | Y          | AGN        | 0.632                         |                              |
| WARPJ2108.6-0507 | rp300389n00           | 21 08 39.9                 | -05 07 27                  | 2.21                               | 3.13                                | 5.57                          | 0.43                          | 1.29          | R          | Y          | CLG        | 0.222                         |                              |

Table 3—Continued

| Name<br>(1)      | ROSAT<br>Field<br>(2) | $\alpha$<br>(J2000)<br>(3) | $\delta$<br>(J2000)<br>(4) | $cr_{raw}$<br>[ $10^{-3}$ ]<br>(5) | $cr_{corr}$<br>[ $10^{-3}$ ]<br>(6) | $n_H$<br>[ $10^{20}$ ]<br>(7) | Flux<br>[ $10^{-13}$ ]<br>(8) | Extent<br>(9) | Im<br>(10) | Sp<br>(11) | Id<br>(12) | Redshift/<br>Sp. Type<br>(13) | Other Name/<br>Notes<br>(14) |
|------------------|-----------------------|----------------------------|----------------------------|------------------------------------|-------------------------------------|-------------------------------|-------------------------------|---------------|------------|------------|------------|-------------------------------|------------------------------|
| WARPJ2157.6–1506 | rp701420n00           | 21 57 40.2                 | –15 06 58                  | 3.67                               | 4.65                                | 3.75                          | 0.6                           | 1.16          | R          | ...        | ...        | ...                           | ...                          |
| WARPJ2224.5–0208 | rp701018n00           | 22 24 31.7                 | –02 08 05                  | 3.01                               | 3.67                                | 4.95                          | 0.49                          | 0.91          | BR         | ...        | ...        | ...                           | ...                          |
| WARPJ2224.6–0218 | rp701018n00           | 22 24 41.2                 | –02 18 26                  | 3.11                               | 4.04                                | 4.95                          | 0.54                          | 1.12          | R          | ...        | ...        | ...                           | ...                          |
| WARPJ2253.9+2911 | rp400293n00           | 22 53 54.5                 | +29 11 46                  | 3.13                               | 3.60                                | 5.68                          | 0.49                          | 1.86          | ...        | Y          | ...        | ...                           | ...                          |
| WARPJ2315.2–0529 | rp300220n00           | 23 15 14.6                 | –05 29 47                  | 3.65                               | 4.24                                | 3.59                          | 0.55                          | 1.08          | R          | ...        | ...        | ...                           | ...                          |
| WARPJ2316.4–0526 | rp300220n00           | 23 16 25.1                 | –05 26 12                  | 3.67                               | 4.61                                | 3.59                          | 0.59                          | 1.16          | R          | ...        | ...        | ...                           | ...                          |
| WARPJ2318.0+1238 | rp200474n00           | 23 18 06.0                 | +12 38 12                  | 3.57                               | 4.23                                | 4.24                          | 0.56                          | 1.06          | R          | ...        | agn        | 0.713                         | RIXOS F294 001               |
| WARPJ2343.4–1443 | rp701205n00           | 23 43 27.6                 | –14 43 02                  | 3.37                               | 4.91                                | 2.2                           | 0.61                          | 1.36          | R          | ...        | ...        | ...                           | ...                          |
| WARPJ2343.4–1500 | rp701205n00           | 23 43 26.3                 | –15 00 51                  | 3.18                               | 4.17                                | 2.2                           | 0.52                          | 1.22          | R          | ...        | ...        | ...                           | ...                          |

Table 4. WARPS-I Statistically Complete, Flux Limited Sample

| Name             | $\alpha$<br>(J2000) | $\delta$<br>(J2000) | Extent | $n_H$<br>[ $10^{20}$ ] | Flux<br>[ $10^{-13}$ ] | $\log L_x$ | $r_c$<br>['] | $z$   | $n_z$ | Flags | Other Name/<br>Notes  |
|------------------|---------------------|---------------------|--------|------------------------|------------------------|------------|--------------|-------|-------|-------|-----------------------|
| (1)              | (2)                 | (3)                 | (4)    | (5)                    | (6)                    | (7)        | (8)          | (9)   | (10)  | (11)  | (12)                  |
| WARPJ0111.6-3811 | 01 11 36.0          | -38 11 08           | 1.63   | 1.78                   | 0.83                   | 42.75      | 18.4         | 0.121 | 3     |       | VMF 009               |
| WARPJ0144.5+0212 | 01 44 30.3          | +02 12 24           | 1.75   | 2.91                   | 1.76                   | 43.34      | 42.5         | 0.165 | 2     |       | VMF 019               |
| WARPJ0206.3+1511 | 02 06 23.7          | +15 11 03           | 1.39   | 6.18                   | 0.86                   | 43.40      | 19.2         | 0.251 | 2     |       | VMF 022, RIXOS        |
| WARPJ0210.4-3929 | 02 10 26.7          | -39 29 27           | 1.76   | 1.43                   | 0.90                   | 43.49      | 39.4         | 0.273 | 2     |       | VMF 025               |
| WARPJ0216.5-1747 | 02 16 32.8          | -17 47 11           | 1.60   | 2.98                   | 1.75                   | 44.41      | 39.1         | 0.578 | 3     | c     |                       |
| WARPJ0228.1-1005 | 02 28 11.7          | -10 05 30           | 1.75   | 2.51                   | 3.23                   | 43.50      | 42.5         | 0.149 | 2     | c     | VMF 026               |
| WARPJ0238.0-5224 | 02 38 01.2          | -52 24 41           | 1.28   | 3.07                   | 5.18                   | 43.62      | 24.8         | 0.135 | 1     |       | A3038, VMF 028, SHARC |
| WARPJ0250.0+1908 | 02 50 03.5          | +19 08 00           | 1.56   | 9.87                   | 1.68                   | 43.05      | 21.2         | 0.122 | 2     |       | SHARC                 |
| WARPJ0348.1-1201 | 03 48 08.7          | -12 01 34           | 1.38   | 3.80                   | 0.97                   | 44.02      | 15.3         | 0.488 | 5     |       |                       |
| WARPJ0951.7-0128 | 09 51 47.0          | -01 28 30           | 1.73   | 3.84                   | 0.73                   | 44.03      | 24.2         | 0.568 | 1     | c     | VMF 076               |
| WARPJ1113.0-2615 | 11 13 05.7          | -26 15 36           | 1.21   | 5.47                   | 0.75                   | 44.26      | 6.7          | 0.725 | 2     |       |                       |
| WARPJ1406.2+2830 | 14 06 16.1          | +28 30 55           | 1.39   | 1.46                   | 0.87                   | 44.07      | 11.8         | 0.546 | ...   |       | VMF 153               |
| WARPJ1406.9+2834 | 14 06 55.4          | +28 34 25           | 1.58   | 1.46                   | 2.25                   | 43.14      | 22.7         | 0.117 | 3     | c     | VMF 154, SHARC        |
| WARPJ1415.1+3612 | 14 15 11.1          | +36 12 03           | 1.36   | 1.14                   | 1.13                   | 44.39      | 11.6         | [0.7] | ...   |       | FIRST                 |
| WARPJ1418.5+2511 | 14 18 31.8          | +25 10 59           | 1.18   | 1.93                   | 6.20                   | 44.37      | 11.9         | 0.296 | 3     |       | VMF 159, SHARC        |
| WARPJ1552.2+2013 | 15 52 12.5          | +20 13 32           | 2.04   | 3.70                   | 3.29                   | 43.43      | 35.7         | 0.135 | 3     |       | VMF 175, SHARC        |
| WARPJ2038.4-0125 | 20 38 29.6          | -01 25 11           | 1.71   | 7.02                   | 0.70                   | 44.17      | 20.3         | 0.679 | 2     |       |                       |
| WARPJ2108.8-0516 | 21 08 51.0          | -05 16 32           | 1.40   | 5.57                   | 1.89                   | 43.93      | 29.7         | 0.317 | 10    |       | VMF 200               |
| WARPJ2239.4-0547 | 22 39 24.8          | -05 47 10           | 1.30   | 4.01                   | 2.88                   | 43.87      | 16.3         | 0.242 | 6     |       | A2465S, VMF 208       |
| WARPJ2239.6-0543 | 22 39 39.6          | -05 43 15           | 1.65   | 4.01                   | 4.04                   | 44.02      | 43.7         | 0.243 | 6     |       | A2465N, VMF 210       |
| WARPJ2302.8+0843 | 23 02 48.1          | +08 43 50           | 0.92   | 4.86                   | 0.72                   | 44.23      | 0.1          | 0.722 | 1     | c     |                       |
| WARPJ2319.5+1226 | 23 19 34.6          | +12 26 21           | 1.42   | 4.42                   | 4.15                   | 43.45      | 28.8         | 0.124 | 3     |       | VMF 217, RIXOS        |

Table 5. WARPS-I Additional Clusters and Candidates

| Name             | $\alpha$<br>(J2000) | $\delta$<br>(J2000) | Extent | $n_H$<br>[ $10^{20}$ ] | Flux<br>[ $10^{-13}$ ] | $\log L_x$ | $r_c$<br>['] | $z$     | $n_z$ | Flags | Other Name/<br>Notes        |
|------------------|---------------------|---------------------|--------|------------------------|------------------------|------------|--------------|---------|-------|-------|-----------------------------|
| (1)              | (2)                 | (3)                 | (4)    | (5)                    | (6)                    | (7)        | (8)          | (9)     | (10)  | (11)  | (12)                        |
| WARPJ0022.0+0422 | 00 22 03.4          | +04 22 38           | 1.81   | 2.87                   | 0.72                   | 43.74      | 28.8         | 0.407   | 5     | 8c    | GHO 00190.5+0405            |
| WARPJ0023.1+0421 | 00 23 06.0          | +04 21 13           | 1.41   | 2.87                   | 0.76                   | 43.86      | 15.6         | 0.453   | 3     | 8     |                             |
| WARPJ0210.2-3932 | 02 10 13.8          | -39 32 50           | 1.77   | 1.43                   | 0.46                   | 42.89      | 19.8         | [0.190] | ...   | <     | VMF 024, estimated redshift |
| WARPJ0234.2-0356 | 02 34 13.3          | -03 56 51           | 1.31   | 2.59                   | 0.64                   | 43.78      | 12.4         | 0.447   | 5     | <     |                             |
| WARPJ0236.0-5224 | 02 36 04.2          | -52 24 50           | 1.09   | 3.08                   | 0.53                   | ...        | 4.2          | ...     | -     | ?     | VMF 027                     |
| WARPJ0255.3+0004 | 02 55 23.1          | +00 04 38           | 1.18   | 6.48                   | 0.64                   | ...        | 5.3          | ...     | -     | ?     |                             |
| WARPJ1407.6+3415 | 14 07 40.5          | +34 15 18           | 1.30   | 1.20                   | 0.58                   | ...        | 11.8         | 0.577   | 1     | ?     |                             |
| WARPJ1415.3+2308 | 14 15 18.4          | +23 08 57           | 1.50   | 1.79                   | 0.57                   | 42.02      | 15.4         | 0.064   | 5     | 8     |                             |
| WARPJ1416.4+2315 | 14 16 26.9          | +23 15 32           | 1.32   | 1.85                   | 12.79                  | 44.02      | 46.1         | 0.137   | 2     | 8c    | SHARC                       |
| WARPJ1501.0-0824 | 15 37 43.0          | +12 01 14           | 0.69   | 7.33                   | 0.49                   | 43.79      | ...          | [0.51]  | -     | ?     | estimated redshift          |
| WARPJ1515.5+4346 | 15 15 31.9          | +43 46 18           | ...    | 1.96                   | ...                    | ...        | ...          | 0.135   | 3     | b     | VMF 169                     |
| WARPJ1517.9+3127 | 15 17 55.9          | +31 27 35           | 1.43   | 1.90                   | 0.57                   | 44.16      | 0.41         | 0.744   | 2     | <     |                             |
| WARPJ1537.7+1201 | 15 37 43.0          | +12 01 14           | ...    | 3.44                   | 1.20                   | 43.01      | ...          | 0.134   | 3     | b     | VMF 171                     |
| WARPJ2108.6-0507 | 21 08 39.9          | -05 07 27           | 1.29   | 5.57                   | 0.41                   | 42.98      | 10.5         | 0.222   | 3     | <     |                             |
| WARPJ2146.0+0423 | 21 46 05.5          | +04 23 13           | 1.33   | 5.42                   | 1.84                   | 44.36      | 20.0         | 0.532   | 4     | 8     | VMF 204, GHO 2143+0408      |
| WARPJ2239.5-0600 | 22 39 35.4          | -06 00 17           | 1.46   | 3.96                   | 0.63                   | 42.95      | 20.2         | 0.174   | 2     | <     | VMF 209                     |
| WARPJ2320.7+1659 | 23 20 46.1          | +16 59 45           | 1.44   | 4.38                   | 0.70                   | ...        | 18.5         | 0.499   | 3     | <c    | AGN (z=1.8)+CLG (z=0.50)    |

Table 6. Radio Sources within 2' of WARPS Cluster Candidates

| Name                | $\alpha$<br>(J2000) | $\delta$<br>(J2000) | Error<br>[""] | Dist<br>[""] | Flux<br>[mJy] | Comments                              |
|---------------------|---------------------|---------------------|---------------|--------------|---------------|---------------------------------------|
| WARPJ0144.5+0212:R1 | 01 44 29.89         | +02 12 43.3         | 1             | 20           | 80.6          | Just north of BCG                     |
| WARPJ0144.5+0212:R2 | 01 44 33.08         | +02 11 41.6         | 4             | 59           | 8.9           |                                       |
| WARPJ0206.3+1511:R1 | 02 06 20.44         | +15 10 56.1         | 1             | 48           | 50.4          |                                       |
| WARPJ0216.5-1747:R1 | 02 16 32.22         | -17 45 17.2         | 3             | 115          | 7.2           |                                       |
| WARPJ0228.1-1005:R1 | 02 28 11.93         | -10 05 32.7         | 4             | 5            | 7.0           | BCG                                   |
| WARPJ0348.1-1201:R1 | 03 48 09.29         | -12 01 59.0         | 1             | 26           | 39.9          | cluster member                        |
| WARPJ0951.7-0128:R1 | 09 51 46.39         | -01 28 32.8         | 4             | 10           | 6.2           | cluster member & star in error circle |
| WARPJ1407.6+3415:R1 | 14 07 45.46         | +34 15 27.2         | 4             | 62           | 0.27          | may be a sidelobe of another source   |
| WARPJ1415.1+3612:R1 | 14 15 10.87         | +36 12 07.0         | 6             | 5            | 5.4           |                                       |
| WARPJ1415.3+2308:R1 | 14 15 18.39         | +23 08 39.6         | 4             | 18           | 8.7           |                                       |
| WARPJ1416.4+2315:R1 | 14 16 27.79         | +23 15 35.3         | 10            | 12           | 4.1           | BCG?                                  |
| WARPJ1418.5+2511:R1 | 14 18 32.57         | +25 12 03.9         | 1             | 65           | 38.9          |                                       |
| WARPJ1501.0-0824:R1 | 15 01 03.22         | -08 24 39.9         | 6             | 23           | 9.6           |                                       |
| WARPJ2038.4-0125:R1 | 20 38 24.76         | -01 24 02.1         | 21            | 100          | 7.9           | Very extended                         |
| WARPJ2038.4-0125:R2 | 20 38 35.49         | -01 25 58.4         | 1             | 100          | 31.1          |                                       |
| WARPJ2108.6-0507:R1 | 21 08 38.81         | -05 07 43.4         | 9             | 22           | 3.7           |                                       |
| WARPJ2108.8-0516:R1 | 21 08 48.87         | -05 16 05.1         | 3             | 41           | 9.6           |                                       |
| WARPJ2146.0+0423:R1 | 21 46 05.92         | +04 22 44.1         | 11            | 30           | 3.6           |                                       |
| WARPJ2239.6-0543:R1 | 22 39 40.32         | -05 43 23.0         | 6             | 14           | 8.4           | BCG                                   |
| WARPJ2302.8+0843:R1 | 23 02 48.10         | +08 43 50.8         | 1             | 0            | 25.6          |                                       |
| WARPJ2320.7+1659:R1 | 23 20 44.42         | +17 00 18.9         | 10            | 41           | 2.8           | background AGN?                       |

This figure "f2\_p1.png" is available in "png" format from:

<http://arxiv.org/ps/astro-ph/0112190v1>

This figure "f3\_p1.png" is available in "png" format from:

<http://arxiv.org/ps/astro-ph/0112190v1>

This figure "f2\_p2.png" is available in "png" format from:

<http://arxiv.org/ps/astro-ph/0112190v1>

This figure "f3\_p2.png" is available in "png" format from:

<http://arxiv.org/ps/astro-ph/0112190v1>

This figure "f2\_p3.png" is available in "png" format from:

<http://arxiv.org/ps/astro-ph/0112190v1>

This figure "f3\_p3.png" is available in "png" format from:

<http://arxiv.org/ps/astro-ph/0112190v1>

This figure "f2\_p4.png" is available in "png" format from:

<http://arxiv.org/ps/astro-ph/0112190v1>

This figure "f3\_p4.png" is available in "png" format from:

<http://arxiv.org/ps/astro-ph/0112190v1>

This figure "f2\_p5.png" is available in "png" format from:

<http://arxiv.org/ps/astro-ph/0112190v1>

This figure "f3\_p5.png" is available in "png" format from:

<http://arxiv.org/ps/astro-ph/0112190v1>

This figure "f2\_p6.png" is available in "png" format from:

<http://arxiv.org/ps/astro-ph/0112190v1>

This figure "f3\_p6.png" is available in "png" format from:

<http://arxiv.org/ps/astro-ph/0112190v1>

This figure "f2\_p7.png" is available in "png" format from:

<http://arxiv.org/ps/astro-ph/0112190v1>

This figure "f3\_p7.png" is available in "png" format from:

<http://arxiv.org/ps/astro-ph/0112190v1>

This figure "f2\_p8.png" is available in "png" format from:

<http://arxiv.org/ps/astro-ph/0112190v1>

This figure "f3\_p8.png" is available in "png" format from:

<http://arxiv.org/ps/astro-ph/0112190v1>

This figure "f2\_p9.png" is available in "png" format from:

<http://arxiv.org/ps/astro-ph/0112190v1>

This figure "f3\_p9.png" is available in "png" format from:

<http://arxiv.org/ps/astro-ph/0112190v1>

This figure "f2\_p10.png" is available in "png" format from:

<http://arxiv.org/ps/astro-ph/0112190v1>

This figure "f3\_p10.png" is available in "png" format from:

<http://arxiv.org/ps/astro-ph/0112190v1>

This figure "f2\_p11.png" is available in "png" format from:

<http://arxiv.org/ps/astro-ph/0112190v1>

This figure "f3\_p11.png" is available in "png" format from:

<http://arxiv.org/ps/astro-ph/0112190v1>

This figure "f3\_p12.png" is available in "png" format from:

<http://arxiv.org/ps/astro-ph/0112190v1>

This figure "f3\_p13.png" is available in "png" format from:

<http://arxiv.org/ps/astro-ph/0112190v1>

This figure "f3\_p14.png" is available in "png" format from:

<http://arxiv.org/ps/astro-ph/0112190v1>

This figure "f3\_p15.png" is available in "png" format from:

<http://arxiv.org/ps/astro-ph/0112190v1>

This figure "f3\_p16.png" is available in "png" format from:

<http://arxiv.org/ps/astro-ph/0112190v1>

This figure "f3\_p17.png" is available in "png" format from:

<http://arxiv.org/ps/astro-ph/0112190v1>

This figure "f3\_p18.png" is available in "png" format from:

<http://arxiv.org/ps/astro-ph/0112190v1>

This figure "f3\_p19.png" is available in "png" format from:

<http://arxiv.org/ps/astro-ph/0112190v1>

This figure "f3\_p20.png" is available in "png" format from:

<http://arxiv.org/ps/astro-ph/0112190v1>